DESIGN, FABRICATION, AND DYNAMIC MODELING OF A PRINTED

CIRCUIT BASED MEMS ACCELEROMETER

Except where reference is made to the work of others, the work described in this thesis is
my own or was done in collaboration with my advisory committee. This thesis does not
include proprietary or classified information.

_____
John E. Rogers

Certificate of Approval:

_____ _____
Ramesh Ramadoss, Co-Chair   John Y. Hung, Co-Chair
Assistant Professor   Professor
Electrical and Computer Engineering   Electrical and Computer Engineering

_____ _____
Bodgan M. Wilamowski   George T. Flowers
Professor   Interim Dean
Electrical and Computer Engineering   Graduate School

DESIGN, FABRICATION, AND DYNAMIC MODELING OF A PRINTED

CIRCUIT BASED MEMS ACCELEROMETER

John E. Rogers

A Thesis

Submitted to

the Graduate Faculty of

Auburn University

in Partial Fulfillment of the

Requirements for the

Degree of

Master of Science

Auburn, Alabama
May 10, 2007

DESIGN, FABRICATION, AND DYNAMIC MODELING OF A PRINTED

CIRCUIT BASED MEMS ACCELEROMETER

John E. Rogers

_____
Signature of Author

_____
Date of Graduation

Vita

John Elvin Rogers was born in Columbus, Georgia in 1982. He grew up in Smiths, Alabama where he graduated from Smiths Station High School in 2002. John then attended Auburn University where he graduated in December 2005 with a Bachelor of Electrical Engineering degree. He then entered graduate school at Auburn University in Spring 2006. His research interests are in nonlinear systems and control, the design and fabrication of Micro-Electro Mechanical Systems (MEMS), Silicon-on-Insulator (SOI) and Printed Circuit Based (PCB) Fabrication Techniques, and monolithic integration of MEMS with electronics. John's interests in MEMS has brought him to study various modeling issues associated with these devices that are still unstudied by engineers.

Thesis Abstract

Design, Fabrication, and Dynamic Modeling of a Printed

Circuit Based MEMS Accelerometer

John E. Rogers

Master of Science, May 10, 2007
(B.E.E., Auburn University, 2005)

76 Typed Pages

Directed by John Y. Hung & Ramesh Ramadoss

A MEMS capacitive-type accelerometer fabricated using printed circuit processing techniques is presented. A Kapton® polymide film is used as the structural layer for fabricating the MEMS accelerometer. The accelerometer proof mass along with four suspension beams are defined in the Kapton® polyimide film. The proof mass is suspended above a RT/Duroid® (Teflon®) substrate using a spacer. The deflection of the proof mass is detected using a pair of capacitive sensing electrodes. The top electrode of the accelerometer is defined on the top surface of the Kapton® film. The bottom electrode is defined in the metallization on the RT/Duroid® substrate. The initial gap height between the bottom electrode and the Kapton® film is approximately 41.8 μm. For an applied external acceleration/deceleration (normal to the proof mass), the proof mass deflects towards or away from the fixed bottom electrode due to inertial force. This deflection causes either a decrease or increase in the air gap height thereby either increasing or decreasing the capacitance between the top and the bottom electrodes.

An example PCB MEMS accelerometer with a square proof mass of membrane area 6.4 mm×6.4 mm is reported. The measured resonant frequency of 375 Hz and the Q-factor in air is 1.5.

The ability to build MEMS accelerometers using low-cost printed circuit processing techniques allows for integration of electronics, suitability for high-volume manufacturing, and large surface area applications for low-g accelerometers. These are all key advantages for using PCB MEMS accelerometers.

Style manual or journal used <u>Journal of Approximation Theory (together with the style</u>
<u>known as "aums").</u>

Computer software used <u>The document preparation package TeX (specifically LaTeX)</u>
<u>together with the departmental style-file `aums.sty`, Microsoft PowerPoint for graphics.</u>

TABLE OF CONTENTS

CHAPTER 1

PCB MEMS ACCELEROMETER

1.1 Background

Micro-Electro-Mechanical Systems (MEMS) is a technology that integrates many engineering fields: electrical, mechanical, materials, computer science, and control systems [1]. MEMS can be classified as either sensors or actuators, and in many applications are a combination of the two. MEMS were first introduced in the early 1960s as discrete open-loop pressure sensors [2]. Typical advantages of MEMS devices include small-size (in the range of 300 nm to 300 μm), light-weight, low-cost, high performance, and low-power consumption [3]. MEMS have found applications in many industries including automotive, biomedical, aerospace, and communications, among many others. MEMS have proven to be a revolutionary technology in many application areas including accelerometers, gyroscopes, pressure sensors, displays, inkjet nozzles, and fluid pumps. Along with the advances in MEMS technology has been a growing interest in the control of MEMS actuators to achieve extended range of motion [4].

In recent years, there has been a considerable interest in development of meso-scale (on the order of $\leq$ 10 mm) MEMS devices fabricated using printed circuit processing techniques known as Printed Circuit Based MEMS or PCB MEMS [5]. In PCB MEMS technology, organic polymer materials are used as substrates, sacrificial layers, and structural layers for fabrication of MEMS devices. PCB MEMS enable monolithic integration of MEMS devices and electronics using low-cost, conventional printed circuit techniques. The advantages of
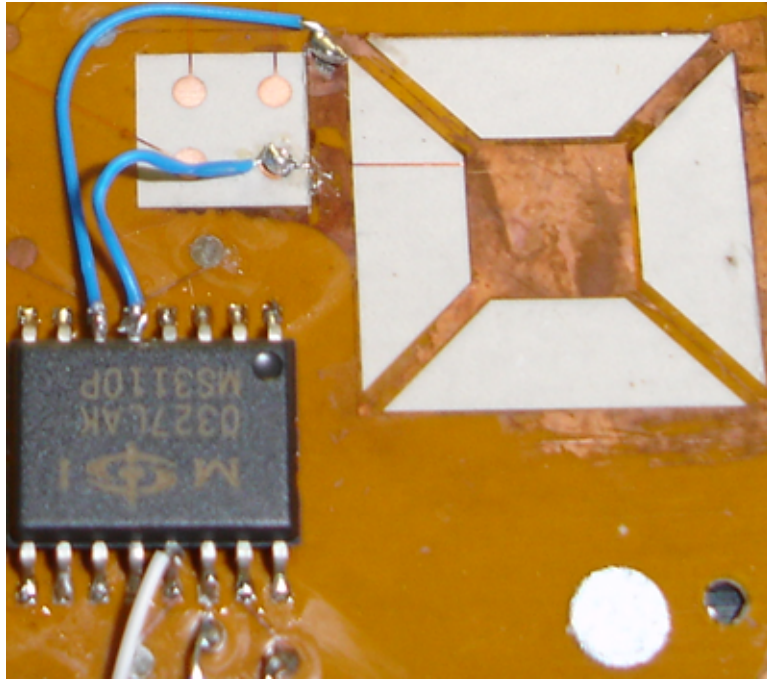
Figure 1.1: Photograph of the fabricated PCB MEMS Accelerometer integrated with capacitive readout chip. Courtesy AMSTC-Auburn University

PCB MEMS components include low-cost, ease of integration with electronics, suitability for high-volume manufacturing, and large surface area applications. Recently, PCB MEMS devices such as flow sensors, tactile sensors [6], pressure sensors [7], salinity sensing system [8], RF MEMS switches [5], and tunable antennas [9] have been demonstrated by various research groups.

One type of PCB MEMS device is known as a PCB accelerometer, shown in Figure 1.1. The accelerometer makes use of organic polymers such as Kapton® film for the structural layer, Polyflon™ bonding film for the spacer layer, and RT/Duroid® (Teflon® for the substrate, as shown in Figure 1.2. The proof mass and its four suspension beams, are defined in the Kapton® polyimide film. A PCB accelerometer is a MEMS-based accelerometer that moves in an out-of-plane motion or a motion orthogonal to the plate mass as shown in

Figure 1.3. An accelerometer can be used to measure acceleration of a moving object as well as velocity and position by integrating electronics. The accelerometer may also be used as a pressure sensor. The ability to build accelerometers using low-cost, conventional printed circuit techniques allows for monolithic integration of MEMS with electronics. Materials, configuration, analysis, fabrication, and experimental characterization of an example PCB MEMS accelerometer are discussed in the following sections.
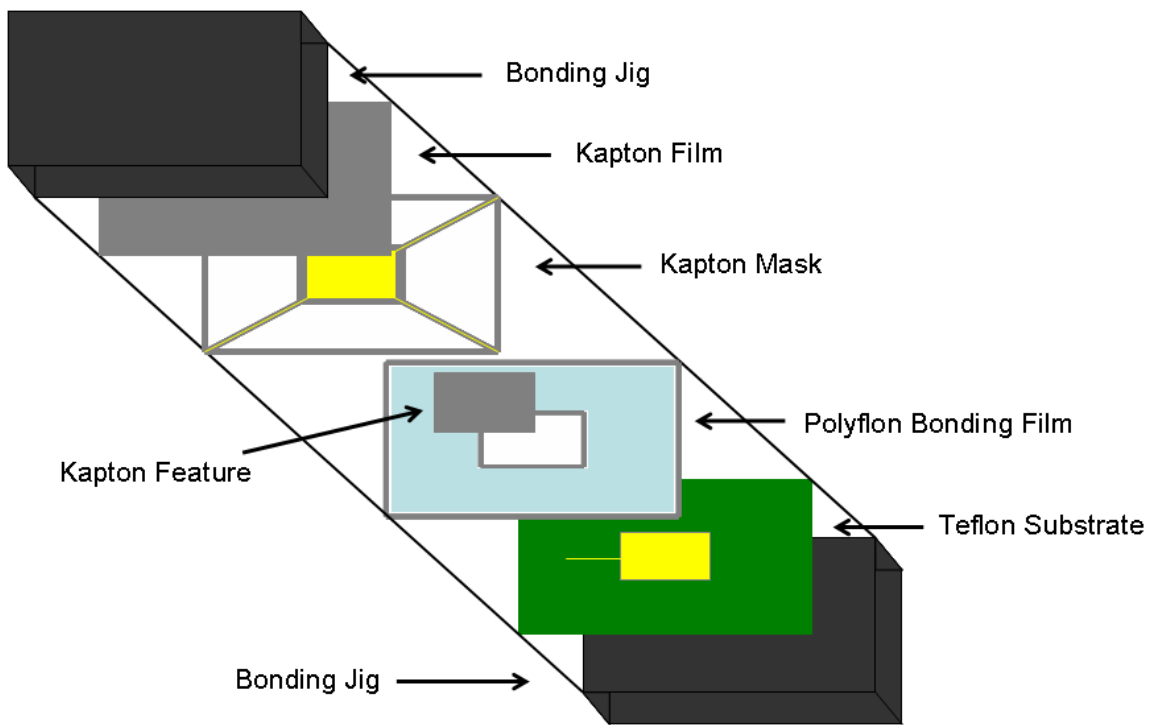
Figure 1.2: Sequence of Layers for PCB MEMS Accelerometer

1.2 Materials, Configuration, & Analysis

The materials, configuration, and analysis of the PCB MEMS accelerometer are discussed in the following subsections. The materials subsection discusses what materials are

used for the PCB MEMS accelerometer. The configuration subsection discusses what the structure is comprised of and how it performs. The analysis subsection discusses the physics behind the structure and how the parameters are derived.
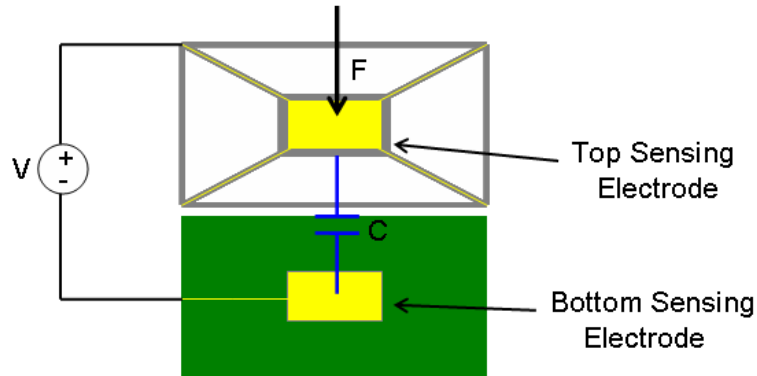
Figure 1.3: Deflection of the PCB MEMS Accelerometer

1.2.1 Materials

The materials used in fabrication of the PCB MEMS accelerometer include Kapton®, Polyflon™, and RT/Duroid® (Teflon®). The Kapton® E polyimide (a polymer of imide monomers) film is available from DuPont and has a permittivity, ϵ_r, of 3.1 at 1 kHz with a 3 μm copper cladding. Kapton® E is a premium performance polyimide film for use as a dielectric substrate in flexible printed circuits and high density interconnects. Kapton® E is a preferred dielectric film for very fine circuitry due to its high modulus and a coefficient of thermal expansion equivalent to that of copper. Kapton® E also has excellent electrical characteristics and chemical etchability. The Polyflon™ bonding film is available from Daikin Industries and is used as a spacer film. Polyflon™ has minimal deformation under loads, is a good electrical insulator (dielectric breakdown strength), and has good

4

transparency. The RT/Duroid® 6002 substrate is available from Rogers Corporation and has a permittivity, $\epsilon_r = 2.94$ at 10 GHz, a dissipation factor, $\tan \delta = 0.0012$ at 10 GHz with a 1/4 oz (9 μm) of copper cladding. RT/Duroid® 6002 is a microwave material with low loss for excellent high frequency performance, extremely low thermal coefficient of dielectric constant, and excellent electrical and mechanical properties.

1.2.2 Configuration

The top and cross-sectional views of the PCB MEMS accelerometer are shown in Fig. 1.4 and Fig. 1.5. The proof mass of the accelerometer is defined in the 2 mil (50.8 μm) thick Kapton® polyimide film. The proof mass comprises of a square membrane supported by four suspension beams. The proof mass is suspended above a 30 mil (762 μm) thick RT/Duroid® substrate using a 2 mil (50.8 μm) thick Polyflon™ bonding film (spacer). For an applied external acceleration/deceleration (normal to the proof mass), the proof mass deflects towards or away from the substrate due to inertial force. The deflection of the proof mass is detected using a pair of capacitive sensing electrodes as shown in Figure 1.3. The top sensing electrode of the accelerometer is defined in the 3 μm thick (standard thickness available from DuPont) copper metallization on the top surface of the Kapton® film. The bottom sensing electrode is defined in the 9 μm thick (standard thickness available from Rogers Corporation) copper metallization on the RT/Duroid® substrate. Standard copper metallization materials available from the manufacturers were used in this work. The top and bottom sensing electrodes have different thicknesses due to the standard thicknesses available from their respective manufacturers. The spacer film determines the nominal air gap height between the Kapton® film and the bottom sensing electrode. The nominal gap
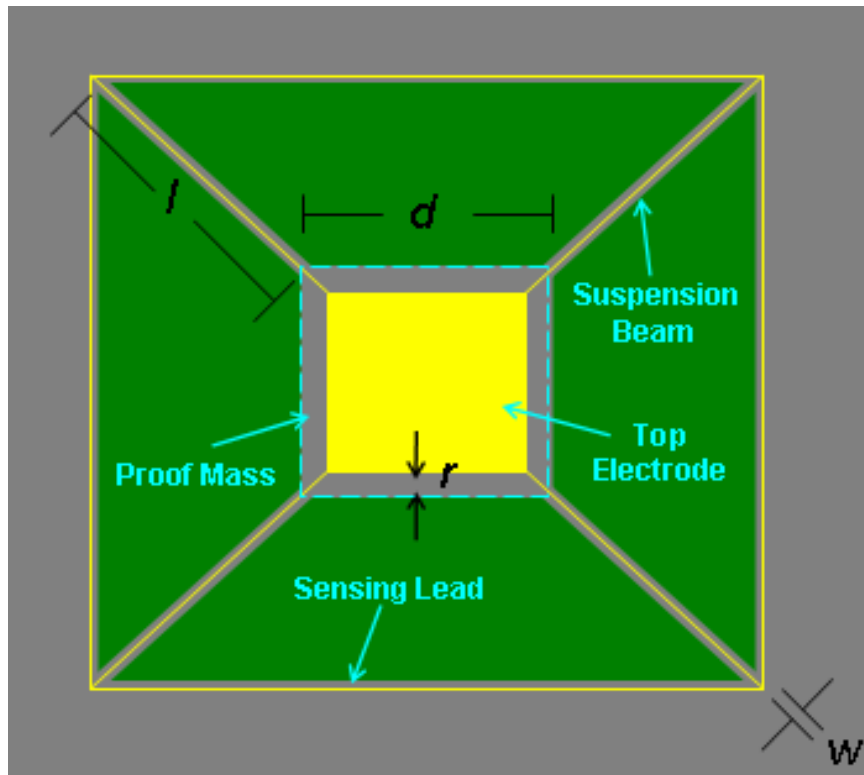
Figure 1.4: Schematic of the PCB MEMS Accelerometer Top view (not to scale)

height is approximately 41.8 μm (50.8 μm spacer - 9 μm bottom sensing electrode). The deflection of the membrane causes either a decrease or increase in the air gap thereby either increasing or decreasing the capacitance between the top and the bottom electrodes. The sensing leads of width 100 μm (chosen by design) are used for connecting the electrodes to the capacitance read-out chip.

1.2.3 Analysis

To understand what's happening dynamically with a MEMS device a knowledge of some basic underlying principles is essential. The electrial and mechanical dynamics of lumped element systems have been studied thoroughly by engineers. The various physical
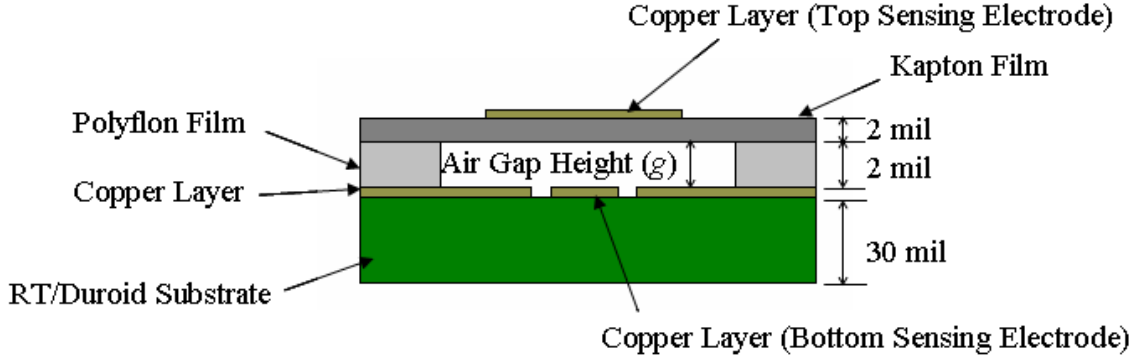
Figure 1.5: Schematic of the PCB MEMS Accelerometer Cross-sectional view (not to scale)

parameters of the PCB MEMS accelerometer are shown in Fig. 1.4 and Fig. 1.5. The area of the square Kapton$^{\circledR}$ membrane is $d \times d$. The length and width of the suspension beams are l and w, respectively. The reduction distance between the square area of the Kapton$^{\circledR}$ membrane and the top electrode is r. In this work, the hypothesis is that the accelerometer may be modeled as a second-order mass-spring-damper system (Appendix A)

$$m\ddot{x} = -c\dot{x} - kx + \frac{\epsilon A V^2}{2} \frac{1}{(g-x)^2} \tag{1.1}$$

where m is the effective mass, c is the damping constant, k is the spring constant, ϵ is the permittivity of the surrounding gas, A is the accelerometer area, V is the applied voltage, and g is the nominal gap distance.

1.3   System Parameters

The estimation of parameters in a system is essential in the analysis process. They can be estimated by knowing information about the geometry, material properties, environmental conditions, etc. If the second-oder model above holds and the parameters can

7

be estimated, a linear state variable control technique can be used to reject disturbrances that would detriment the accelerometer (Appendix C). Some of the system parameters of the example PCB MEMS accelerometer along with their corresponding values are shown in Table 1.1. These parameter values (proof mass, spring consant, damping constant, natural frequency) along with a few others will be derived below.

Table 1.1: Designed System Parameters for the Example PCB MEMS Accelerometer

Parameter	Name	Value	Units
m	effective mass	4.499×10^{-6}	kg
k	spring constant	20.32	N/m
c	damping constant	18.21×10^{-2}	N-sec/m
f_o	natural frequency	338	Hz
g	gap distance	41.8	μm

1.3.1 Spring Constant

The mechanical spring constant for a system is defined by the geometry and materials properties of the spring. A system is usually designed around known spring types (i.e. cantilever beams, fixed-fixed beams), load types (i.e. uniform loads, point loads), and materials (i.e. silicon, Kapton$^{®}$) for ease of calculations. This allows for ease of estimation when designing. It should be noted that the ability to estimate the spring constant allows for the calculation of other unknown parameters (i.e. damping) in the experimental results. The spring constant for the given accelerometer has four cantilever beams with distributed point loads (Figure 1.4).

The spring constant of the bi-material Kapton®-copper suspension beams of the accelerometer is given by

$$k = \frac{48EI}{l^3} \qquad (1.2)$$

where EI is the equivalent flexural rigidity [10] given by

$$EI = \frac{(w_c E_c t_c^2)^2 + (w_k E_k t_k^2)^2 + 2w_c w_k E_c E_k t_c t_k (2t_c^2 + 3t_c t_k + 2t_k^2))}{12(w_c E_c t_c + w_k E_k t_k)} \qquad (1.3)$$

where E_k and t_k are the Young's modulus and thickness of the Kapton® film, E_c and t_c are the Young's modulus and thickness of copper, w_k and w_c are the widths of the Kapton® and copper in the suspension beams, and l is the length of the suspension beams.

1.3.2   Proof Mass

The effective mass, or proof mass, is the total mass that will experience motion as a result of an inertial force. On the accelerometer the plate mass will displace, but there is also spring displacement. For any one spring, a fraction of the spring mass will displace from one end of the pinned or fixed side. The question then arises of how much of the spring will displace? This can be calculated using the Rayleigh-Ritz Method [11] for vibration frequency. The Rayleigh-Ritz Method is based on the principle of energy conservation and is used for calculating the vibration frequency of systems with distributed masses. Experimentally, the distributed mass can be solved for if one knows the vibration frequency and the spring constant. The Rayleigh-Ritz Method for the accelerometer is solved for in

9

Appendix B. The results from the Rayleigh-Ritz Method show the effective proof mass is

$$m = m_p + \frac{13}{35}m_b \qquad (1.4)$$

where m_p is the mass of the Kapton® membrane with the copper top electrode and m_b is the total mass of all four suspension beams (along with sense leads).

1.3.3 Natural Frequency

The vibration frequency, or natural frequency, is the frequency at which a device naturally vibrates or oscillates. The accelerometer should be operated below this frequency (in other words the accelerometer must be shaken below this frequency) in order to operate as an accelerometer. The natural frequency of the accelerometer can be expressed

$$\omega_o = \sqrt{\frac{k}{m}} \qquad (1.5)$$

where k is the effective spring constant and m is the effective proof mass of the accelerometer.

1.3.4 Damping Constant

The accelerometer moves in an out-of-plane motion or a motion orthogonal to the plate mass. Squeeze-film damping is the dominant damping mechanism in this configuration. The squeeze-film damping refers to the energy dissipated in displacing the gas molecules between the moving beam or plate and the substrate. The squeeze-film damping constant

for a square membrane [11] is

$$c = \frac{0.42 \mu d^4}{g^3} \tag{1.6}$$

where μ is the viscosity of air (= 18.27 μPa.s at 20°C), d is the side length of the plate mass (Kapton® film), and g is the nominal gap height between the bottom electrode and the Kapton® film.

1.3.5 Quality Factor

The quality factor is a measure of how well a system dissipates energy. The quality factor is defined as the energy stored over the power loss at resonance. Thus a higher quality factor indicates a lower rate of energy dissipation at resonance. The quality factor, Q, of the accelerometer is given by

$$Q = \frac{\omega_o m}{c} \tag{1.7}$$

where ω_o is the resonant frequency, m is the proof mass, and c is the damping constant of the accelerometer.

In this work, an example PCB MEMS accelerometer with a square membrane of area 6.4 mm×6.4 mm is considered. The length l and width w of the suspension beams are 5.8 mm and 1 mm, respectively. The reduction distance between the square area of the Kapton® membrane and the top electrode is 270 μm. The initial gap height g is approximately 41.8 μm. These parameter values were chosen based on using equations (2.2)-(2.7) to design an accelerometer with a low-frequency resonance for low-g applications. This

means that the spring to mass ratio given by Equation (2.5) should be small. The various system parameters can be calculated and are shown in Table 1.1. In the following sections, fabrication and experimental characterization are discussed.

1.4   Fabrication

The PCB accelerometer is fabricated using printed circuit techniques. The fabrication of the accelerometer has three layers: a substrate layer, spacer layer, and polyimide layer (Figure 1.5). They will be discussed in further detail below. The substrate layer is made of RT/Duroid®, a Teflon® material. The spacer is made of a Polyflon™ bonding layer. The polyimide layer is made of Kapton® film.

1.4.1   Substrate

The substrate chosen is a 30 mils (762 μm) thick RT/Duroid® with 9 μm thick copper metallization. The bottom electrode for capacitive sensing is defined in the copper metallization on the RT/Duroid® substrate.

1.4.2   Spacer

The spacer layer provides the required spacing between the substrate and the Kapton® polyimide layer. Hence, the thickness of the spacer film determines the up-position gap height. A 2 mil (50.8 μm) thick Polyflon™ bonding film is used as the spacer layer. The bonding film was cut to create openings for the movable membrane with suspension beams. A milling machine could be employed for designs with small characteristic dimensions.

1.4.3 Kapton® Film

A 2 mil (50.8 μm) thick Kapton® film with 3 μm thick copper metallization is used as the structural layer for the accelerometer. The Kapton® film contains copper metallization on both sides as shown in Figure 1.6. A 150-250Å thick nichrome seed layer is present between the Kapton® film and the copper layer. The film is essentially a sandwich of copper-nichrome-kapton-nichrome-copper. The two major steps in the fabrication of the Kapton® film are discussed in detail below.

Figure 1.6: A 2 mil thick Kapton® film used for fabrication of the PCB MEMS Accelerometer

Plasma Etching of Kapton® Film

Fabrication starts with rinsing of the Kapton® film using Acetone then Methanol followed by cleaning using diluted sulfuric acid to remove any oxide growth on the copper surfaces. The bottom side copper is used to define the mask for DRIE processing. A piece of Dynaflex wafer grip film is attached to a silicon wafer by heating it on a hotplate to 110^oC. The Dynaflex wafer grip film is used as an adhesion layer to mount the Kapton® film to the wafer. When the wafer is sufficiently hot (110^oC), the Kapton® is carefully attached by hand to the wafer in a way as to smooth out all air pockets. The next step is

13

to spin-coat photoresist (PR) onto the Kapton® film and soft bake. The Kapton® film is then exposed and developed using the Kapton® layer mask.

The copper is then etched off using an industry standard copper etchant such as CE-200. The photoresist is then removed and the nichrome is fully etched off from the Kapton® layer pattern. The wafer is then ready for the Deep Reactive Ion Etch (DRIE) process. The wafer is put into the DRIE where the etcher will etch through the Kapton® and nichrome/copper on the back side. The equipment used for the DRIE process is an STS AOE (Advanced Oxide Etcher). The configuration of the gases used for this etch in Auburn University's AMSTC facility is 8 sccm carbon tetrafluoride (CF_4) and 35 sccm oxygen with 500 Watts of radio frequency (RF) power. Using these processing parameters it takes about 70 minutes to etch a 2 mil thick Kapton® layer. The bottom copper and nichrome are etched fully using chemical etchants. Then, the wafer grip is dissolved using Amyl Acetate and the Kapton® film is removed by hand from the wafer.

Top Electrode Patterning

At this stage, the Kapton® film contains copper and nichrome layers on only one side. The Kapton® side is then attached to the dicing tape. The film is then attached to a silicon wafer and photoresist is spin-coated. The top sensing electrode mask is used to define the top electrode in the copper layer on the Kapton®. Finally, the nichrome is removed.

Thermal Compression Bonding

Thermo-compression bonding is performed using a Carver Press consisting of two platens. The platens are heated using heaters, whose temperature is sensed by a thermocouple. The fixture consists of two steel plates with alignment holes on them. The

14

substrate forms the bottom most layer, the spacer is the middle layer and the Kapton$^{\circledR}$ film forms the top most layer in this structure. The different layers are aligned by aligning the holes created on the three layers during the fabrication process described earlier. This unit is now placed between the press platens. The bonding is performed at a pressure of 80 psi (a load of 200 lbs.) and a temperature of 130°C. Both pressure and temperature are maintained for 5 min during bonding. Before pressure is released, the assembly is cooled down to the room temperature in a process known as annealing.

1.5 Detailed Fabrication Process

Table 1.2: PCB MEMS Accelerometer

Process	Method	Time
	Kapton Film Cleaning	
1. Cleaning	Acetone then Methanol	
	DI Rinse	30 Sec
	N_2 Dry	
2. Oxide Removal	250mL of H_2O + 2 drops of H_2SO_4	
	DI Rinse	30 Sec
	N_2 Dry	
3. Cleaning	Acetone then Methanol	
	DI Rinse	30 Sec
	N_2 Dry	
	Stick Kapton Film on Wafer	
1. 4" Wafergrip Application	Apply Wafergrip on wafer	
2. Soft Bake	Hot plate - 110°C	30 Sec
3. Stick Film on Wafer	Smooth Kapton Film on wafer	

	Define Kapton Layer	
1. Spin Photoresist	S1813 Photoresist	30 Sec
		2500 RPM
		500 r/s ramp
2. Soft Bake	Hot plate - 110°C	60 Sec
3. UV Exposure	Mask Aligner - expose Kapton Layer mask	30 Sec
4. Develop	CD-30 developer	45 Sec
	DI Rinse	30 Sec
	N_2 Dry	
5. Hard Bake	Hot plate - 110°C	60 Sec
6. Wet Etch	CE-200 etchant	8 Sec
	DI Rinse	30 Sec
	N_2 Dry	
7. Remove Photoresist	Acetone then Methanol	
	DI Rinse	30 Sec
	N_2 Dry	
8. Wet Etch	NaOH + $KMNO_4$ mixture	50 Sec
	DI Rinse	30 Sec
	N_2 Dry	
9. Cleaning	Acetone then Methanol	
	DI Rinse	30 Sec
	N_2 Dry	
	Deep Reactive Ion Etch (DRIE)	
1. DRIE	4:1 CF_4:O_2 proces	75 Min
2. Cleaning	Acetone then Methanol	
	DI Rinse	30 Sec
	N_2 Dry	
3. Remove/Clean Kapton Film	Remove Kapton Film from Wafer Clean using Amyl Acetate	
4. Cleaning	Acetone then Methanol	
	DI Rinse	30 Sec
	N_2 Dry	

	Define CopperTop Layer	
1. Spin Photoresist	S1813 Photoresist	30 Sec
		2500 RPM
		500 r/s ramp
2. Soft Bake	Hot plate - 110°C	60 Sec
3. UV Exposure	Mask Aligner - expose CopperTop mask	1:30 Min
4. Develop	CD-30 developer	45 Sec
	DI Rinse	30 Sec
	N$_2$ Dry	
5. Hard Bake	Hot plate - 110°C	60 Sec
6. Wet Etch	CE-200 etchant	8 Sec
	DI Rinse	30 Sec
	N$_2$ Dry	
7. Remove Photoresist	Acetone then Methanol	
	DI Rinse	30 Sec
	N$_2$ Dry	
8. Wet Etch	NaOH + KMNO$_4$ mixture	50 Sec
	DI Rinse	30 Sec
	N$_2$ Dry	
9. Cleaning	Acetone then Methanol	
	DI Rinse	30 Sec
	N$_2$ Dry	
	Define Subini Layer	
1. Cleaning	Acetone then Methanol	
	DI Rinse	30 Sec
	N$_2$ Dry	
2. Oxide Removal	250mL of H$_2$O + 2 drops of H$_2$SO$_4$	
	DI Rinse	30 Sec
	N$_2$ Dry	
3. Cleaning	Acetone then Methanol	
	DI Rinse	30 Sec
	N$_2$ Dry	
4. Tape RT/Duroid	Apply blue tape to one side of RT/Duroid	
5. Spin Photoresist	S1813 Photoresist	30 Sec
		2500 RPM
		500 r/s ramp
6. Soft Bake	Hot plate - 110°C	60 Sec

|		
7. UV Exposure	Mask Aligner - expose Subini mask	30 Sec
8. Develop	CD-30 developer	45 Sec
	DI Rinse	30 Sec
	N_2 Dry	
9. Hard Bake	Hot plate - 110°C	60 Sec
10. Wet Etch	CE-200 etchant	8 Sec
	DI Rinse	30 Sec
	N_2 Dry	
11. Remove Photoresist	Acetone then Methanol	
	DI Rinse	30 Sec
	N_2 Dry	
	Define Subcop Layer	
1. Cleaning	Acetone then Methanol	
	DI Rinse	30 Sec
	N_2 Dry	
2. Spin Photoresist	S1813 Photoresist	30 Sec
		2500 RPM
		500 r/s ramp
3. Soft Bake	Hot plate - 110°C	60 Sec
4. UV Exposure	Mask Aligner - expose Subcop mask	30 Sec
5. Develop	CD-30 developer	45 Sec
	DI Rinse	30 Sec
	N_2 Dry	
6. Hard Bake	Hot plate - 110°C	60 Sec
7. Wet Etch	CE-200 etchant	8 Sec
	DI Rinse	30 Sec
	N_2 Dry	
8. Remove Photoresist	Acetone then Methanol	
	DI Rinse	30 Sec
	N_2 Dry	
9. Wet Etch	NaOH + $KMNO_4$ mixture	50 Sec
	DI Rinse	30 Sec
	N_2 Dry	
10. Cleaning	Acetone then Methanol	
	DI Rinse	30 Sec
	N_2 Dry	

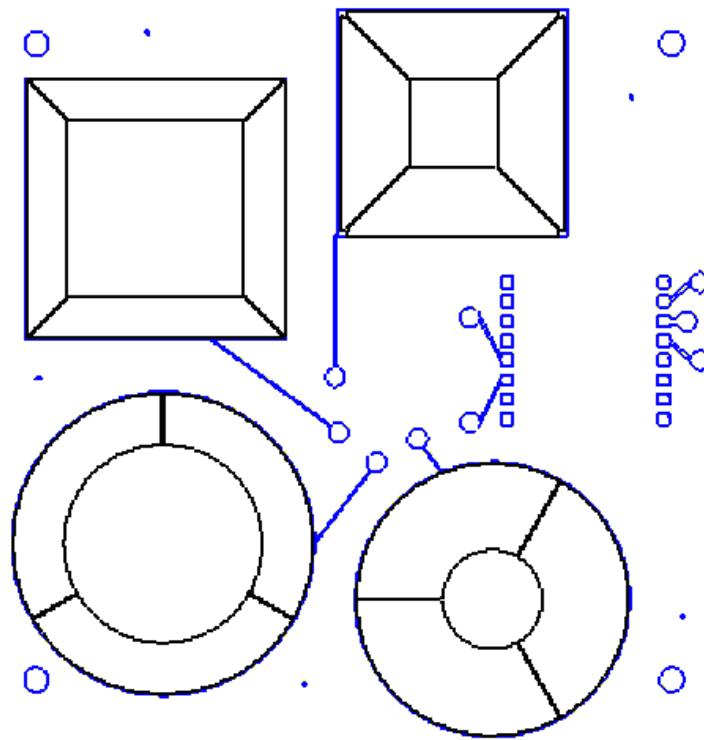## 1.6   Photolithography Masks
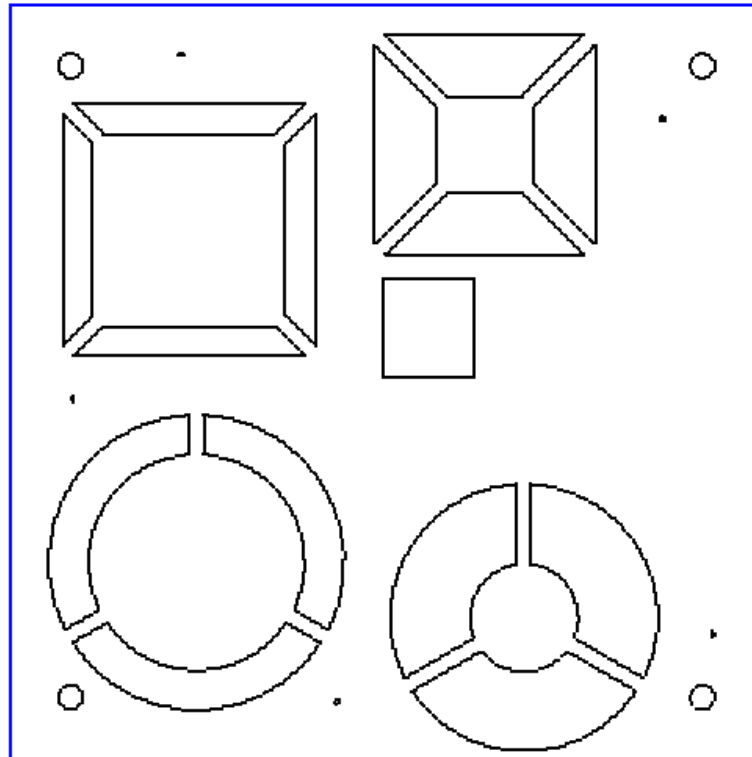
Figure 1.7: Kapton Mask used in Photolithography

Design 1 Coppertop

Figure 1.8: CopperTop Mask used in Photolithography
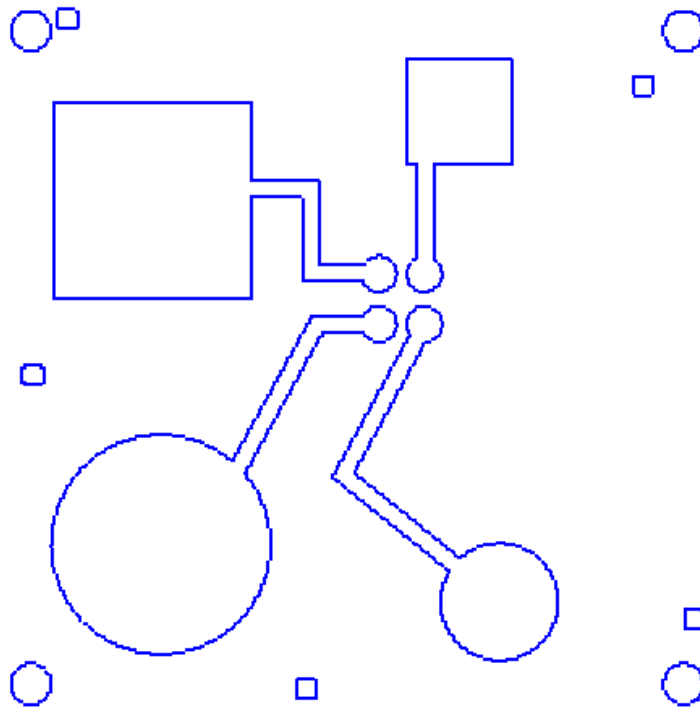
Figure 1.9: Subini Mask used in Photolithography
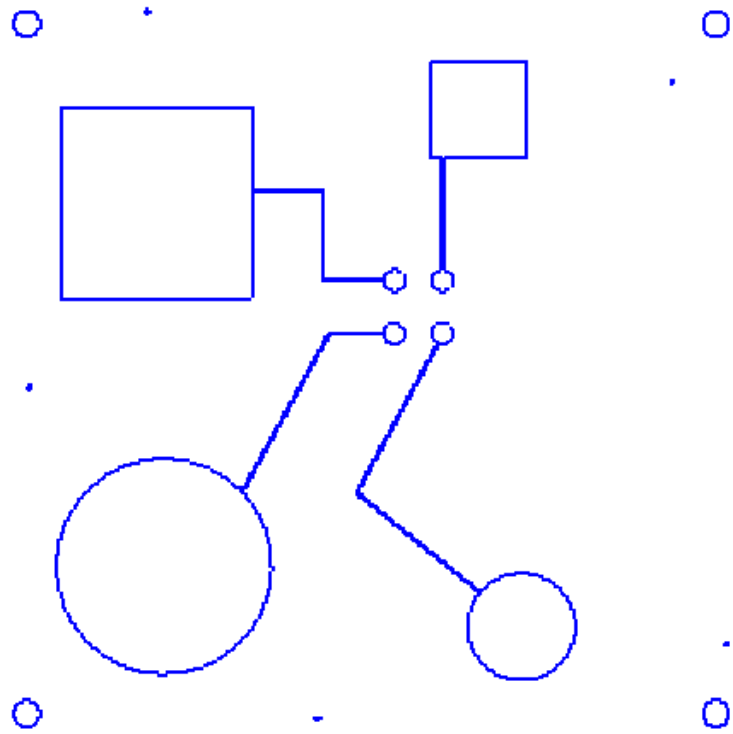
Figure 1.10: Subcop Mask used in Photolithography

1.7 Fabrication Issues

Fabrication of a PCB MEMS accelerometer raises many issues. Some of the fabrication issues can be attributed to the fabrication equipment. For example, fine temperature control and pressure control are hard to achieve. If a process calls for a specific temperature and pressure to be maintained over a time period, then undesirable results could be formed and cause further defects in other fabrication steps. There can also be issues with the chemicals used. For example, if a certain chemical is used as an etchant and has been used for several cycles, then the etchant will not etch at the same rate and if the time is kept constant the result will be an unfinished surface. This issue occured in all of the chemical processes due to recycling of the chemicals and was delt with by overetching until it was visibly clear that the process was done. The environmental conditions such as temperature, pressure, moisture can also effect the chemicals, but are usually controlled in a microfabrication clean room.

Scattering of the copper layer is another issue in fabrication. Scattering means the copper layer begins to crack and break under the high temperatures present in the DRIE process. This happens due to the large difference in thermal coefficients of expansion between copper and Kapton®. This issue wasn't considered before fabrication, thus the fabrication steps were altered to use the backside of the Kapton® film for the copper layer. To avoid this issue for top and backside copper metallizations aluminum must be deposited before DRIE and removed after DRIE.

Residual stress is another possible issue in printed circuit techniques due to the combination of Kapton® with nichrome and copper. Residual stress occurs when a thin film is deposited on a substrate and has in-plane stress. Plane stress is caused by mismatches

in thermal expansion of the film and sustrate, which can lead to deformation of the device. This happened when the various layers were pressure bonded in the thermo-compression bonding stage. The gap increased and warped due to these mismatches. These effects could have been supressed by having copper layers on both sides of the Kapton® to even out the mismatches.

Another issue with Kapton® is the fact that it is a thin polyimide film. This means that every process that requires the film to be moved by hand carries with it the potential to bend the film and make permanent dents thus creating further warpage of the film. This has the potential to happen in the chemical etching stages where the Kapton® film must be moved back and forth with wafer tweezers in order for the etchant to be effective. There is also the potential for warping in the drying of the Kapton® film. Every time the Kapton® film is cleaned or etched it must go through deionized water then dried with nitrogen (N_2) gas. The N_2 gas has a high pressure rate and when spread across the Kapton® film has the potential to create dents. These fabrication issues can and do effect the modeling of the device as they will change the various parameters (i.e. mass, spring constant).

CHAPTER 2

EXPERIMENTAL CHARACTERIZATION

2.1 Experimental Set-up

A photograph of the fabricated MEMS accelerometer is shown in Fig. 2.2. The MEMS accelerometer was characterized using an LDS model V408 electromechanical shaker shown in Figure 2.1. For testing purposes, the accelerometer substrate was mounted onto a plexiglass fixture as shown in Figure 2.2 with a mounting screw attached at the center of the bottom surface. The plexiglass is attached to the threaded hole in the shaker head. The shaker vibrates the MEMS accelerometer at a chosen amplitude over a specified frequency range. In response to the applied external acceleration/deceleration, the proof mass vibrates in a direction normal to the substrate.

The mechanical displacement of the proof mass was measured by reflecting a laser beam off of the proof mass using a laser interferometric measurement system as shown in Figure 2.3. The experiment yields $y(f)$, the motion of the membrane as a function of frequency. The Teflon$^{\circledR}$ substrate was used as a reference frame and a second laser interferometric measurement system was used to measure the motion of the reference frame as a function of frequency, $x(f)$, by reflecting a laser beam off of the reference frame. The signals $x(f)$ and $y(f)$ were recorded simultaneously using a signal analyzer. The signal analyzer provides the transmissibility spectrum of the MEMS accelerometer by computing the transfer function $T(f) = y(f)/x(f)$. The transmissibility spectrum is defined as the ratio of the magnitudes of the displacement of the membrane (output) and the reference frame (input) over a range of frequencies otherwise known as the transfer function.

Figure 2.1: A Photograph of an LDS model V408 electromechanical shaker (courtesy Auburn University).

2.2   Experimental Results

The measured magnitude of the transfer function as a function of frequency for the PCB MEMS accelerometer is shown in Figure 2.4. From this plot, the resonant frequency and the quality factor of the MEMS accelerometer were found to be 375 Hz and 1.5, respectively. The measured resonant frequency is reasonably close to that of the calculated value of 338 Hz (refer Table 1.1). The measured Q is higher than that of the estimated value due to a larger air gap height caused by the thermal expansion of various layers in the accelerometer during fabrication. Using Equation (2.6), the effective air gap height can be estimated to be 125 μm.
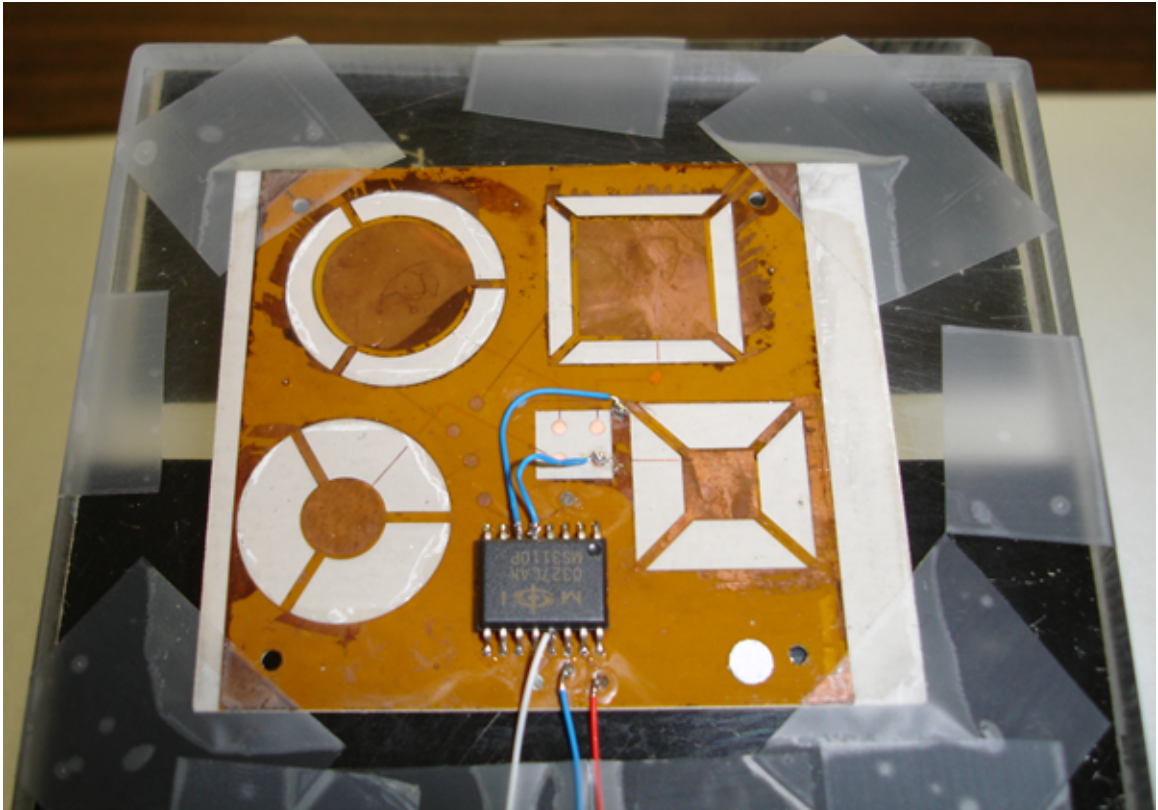
Figure 2.2: Full photograph of PCB MEMS Accelerometer. Courtesy AMSTC-Auburn University

The first experimental results for the PCB MEMS accelerometer were taken using the set-up described above using two lasers to measure the displacements of both the membrane and the reference frame. The mechanical results for this set-up are shown in Figure 2.4. The second experimental results were taken of the electrical characteristics as well as more mechanical characteristics. The electrical characteristics were taken by having the input signal be the reference frame and the output signal be the electrical output from the capacitance to voltage or C-V chip. The C-V chip detects a capacitance from the accelerometer and converts it to a voltage in by a linear amount (1 V/pF) and the output is that amount added to a bias voltage of approximately 2.25 V. The change in deflection of the membrane
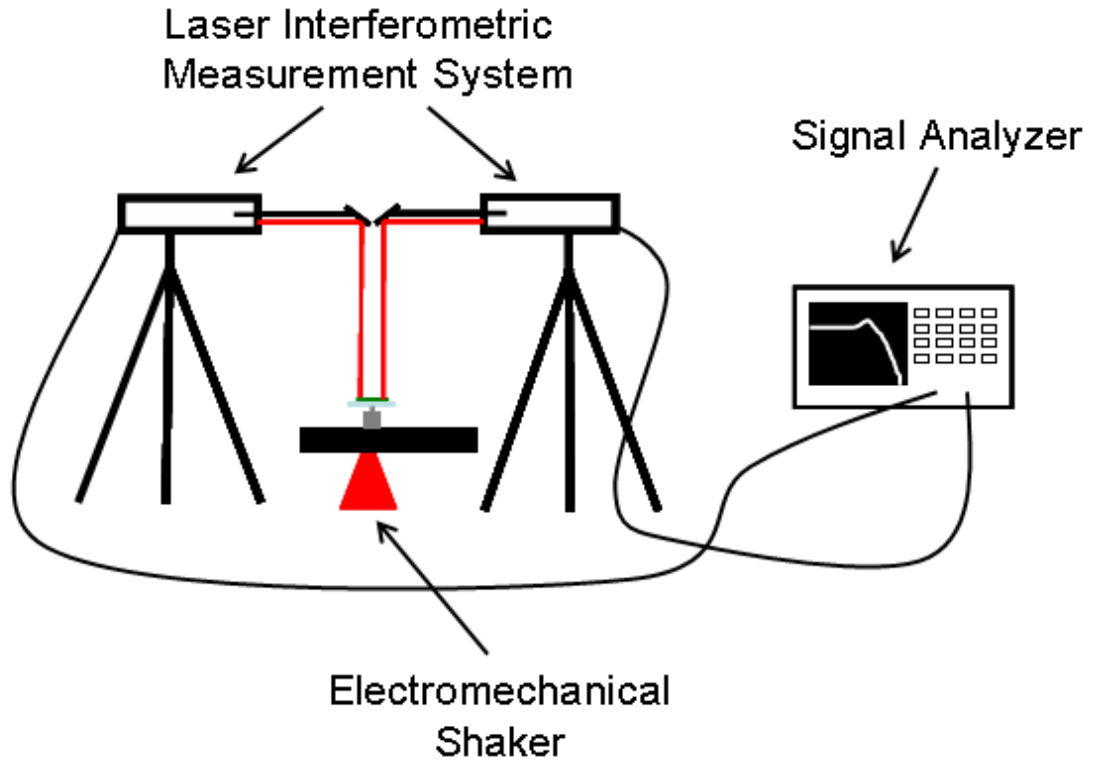
Figure 2.3: Laser Interferometric Measurement System

creates a change in capacitance which results in a voltage change. The signal analyzer then creates a transfer function of the output voltage over the reference frame displacement.

$$C = \frac{\epsilon A}{g} \tag{2.1}$$

$$\frac{\partial C}{\partial g} = -\frac{\epsilon A}{g^2}\dot{g} \tag{2.2}$$

$$V_{out} = V_{bias} + C(\frac{1V}{1pF}) \tag{2.3}$$

For low frequency there's a small change in displacement, $\dot{g}$, which results in a small change in capacitance. The bias voltage, V_{bias}, falls out in the transfer function and only the voltage
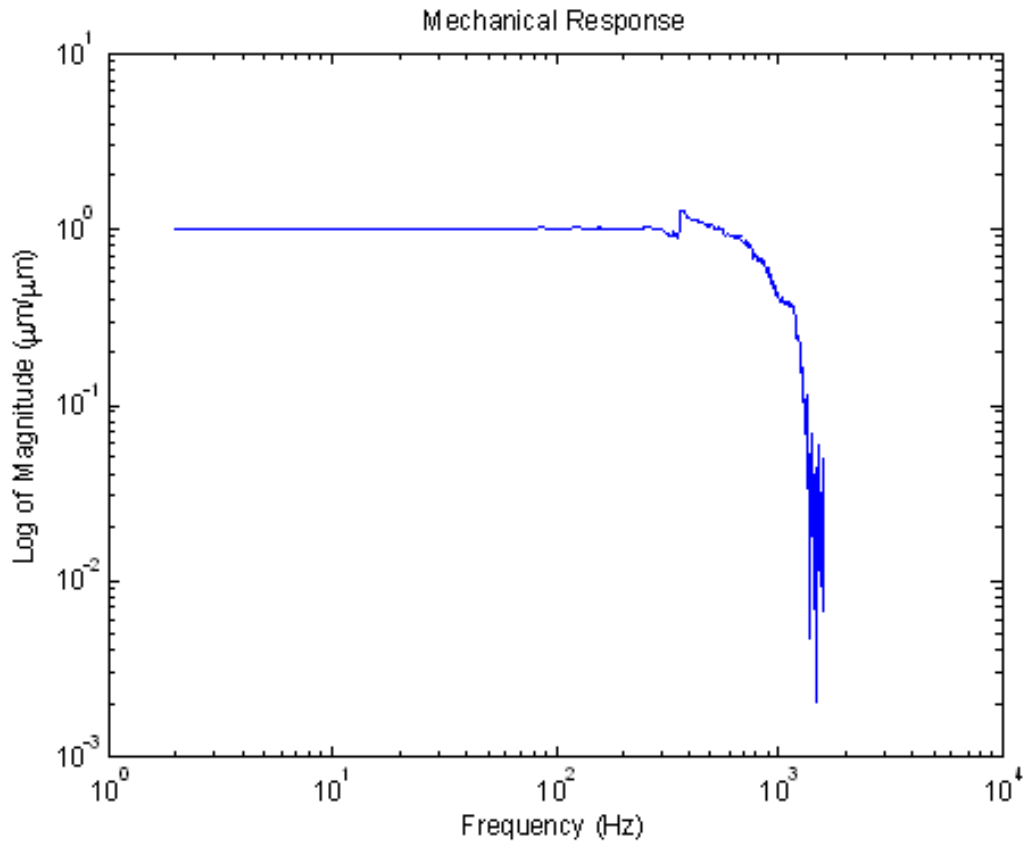
Figure 2.4: Magnitude Plot of the Transfer Function for the PCB MEMS Accelerometer (First Test, Mechanical Response)

due to capacitance change is considered. The electrical results for this set-up are shown in Figure 2.5. The results show a linear increase in voltage of 20dB/decade for low frequency. The plot then rolls off due to the mechanical response.

The mechanical characteristics were taken in the same set-up as the first experimental results. There are three plots shown in Figure 2.6 that represent three measurements taken over the membrane at various positions for statistical purposes. These plots were taken by the signal analyzer over a long period of time to insure a sufficiently rich set of data for statistical analysis. The results were taken on a different day and match up with the results

Figure 2.5: Magnitude Plot of the Transfer Function for the PCB MEMS Accelerometer (Second Test, Electrical Response)

taken in the first experiment and thus show the experimental results are replicable. Note however that these results are not ensured for replicated fabrication due to the fabrication issues described in Section 1.5

The results show a resonant frequency around 375 Hz. The results also show a quality factor or Q factor of 1 to 1.5. These results vary from those seen in Table 1.1. By closer inspection of Figure 1.1 it can be seen that the amount of copper left on the beams is much more than that shown in Figure 1.4. This will change the spring constant as well as the effective mass. By using the WYKO Profiler in Auburn University's CAVE lab it was
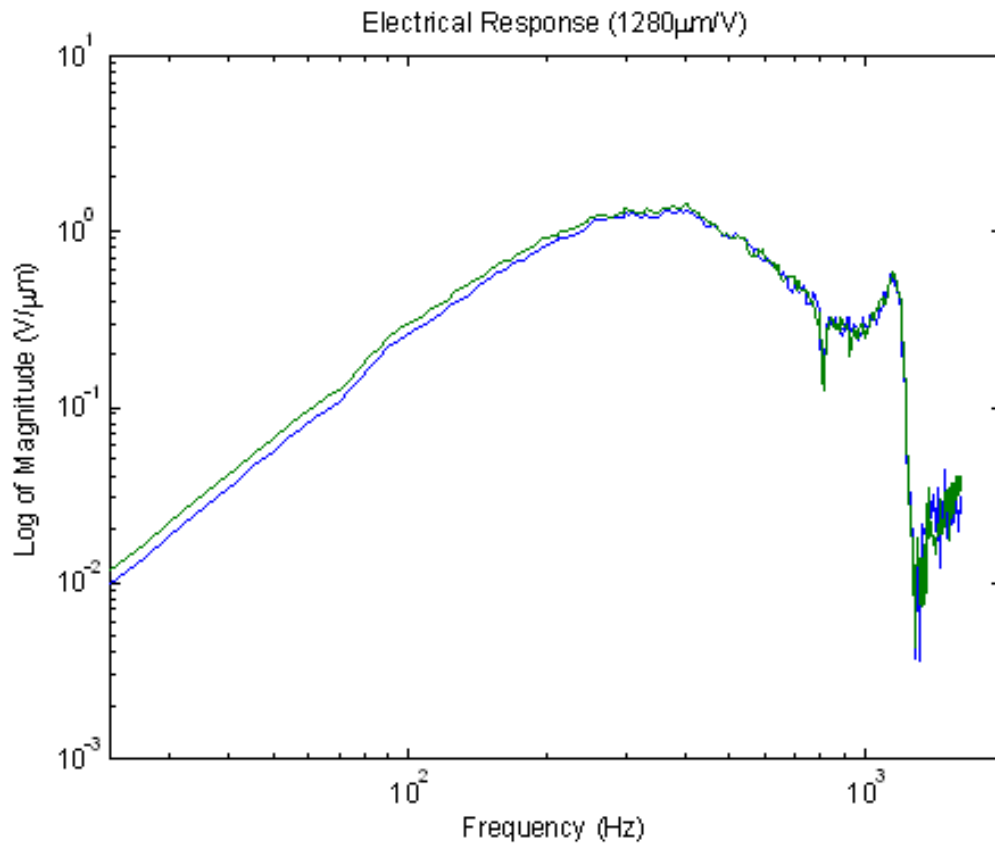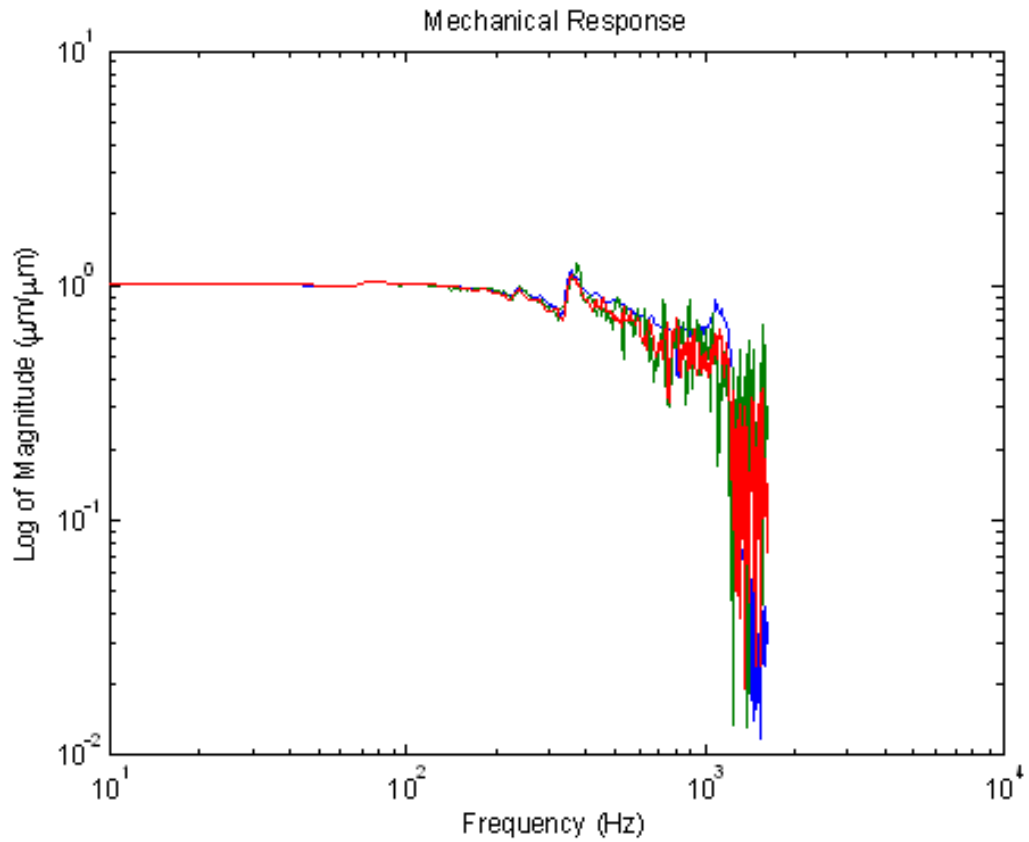
Figure 2.6: Magnitude Plot of the Transfer Function for the PCB MEMS Accelerometer (Second Test, Mechanical Response)

observed that the plate was warped and the actual gap distance could not be calculated. A distributed gap then had to be calculated to represent the overall warpage and was calculated to be 125 μm. This gap is more than three times that of the original gap. This mismatch can be explained by the thermal compression stage of fabrication. PCB devices will experience an expansion in the gap distance due to thermal compression due to mismatches in thermal coefficients of copper and Kapton® [12]. These changes due to fabrication will change the system parameters as shown in Table 2.1.

Table 2.1: Actual System Parameters for the Example PCB MEMS Accelerometer

Parameter	Name	Value	Units
m	effective mass	4.499×10^{-6}	kg
k	spring constant	24.93	N/m
c	damping constant	6.8×10^{-3}	N-sec/m
f_o	natural frequency	375	Hz
g	gap distance	125	μm

There also is seen in the frequency results a second resonant frequency around 1100 Hz in some of the results. In the ideal case the accelerometer would move only in an out-of-plane motion. This resonant frequency may correspond to a torsional motion. Torsional motion has the potential to excite other higher frequency harmonics. There also is a dip before the resonant frequency that may be associated with under-damping. The accelerometer doesn't seem to have a second-order model as described in Section 1.2.3. As to be described in the following section, the accelerometer seems to fit better with a higher-order model. This is most likely due to the accelerometer having more of a flexible structure than a hypothesized rigid structure. Rigid structures can more accurately be described with second-order models, but flexible structures have more of a wave-like nature to them. Flexible structures can thus better be described with distributed parameters rather than lumped-element parameters. The torsional motion notion helps supplement this argument. The quick roll-off at frequencies above the second resonant frequency also seems to support a higher-order model. The accelerometer with the given actual parameters in Table 2.1 should have a second-order response seen in Figure 2.7, but it is obvious that the system has a higher-order response. These issues will be further discussed in the next section.
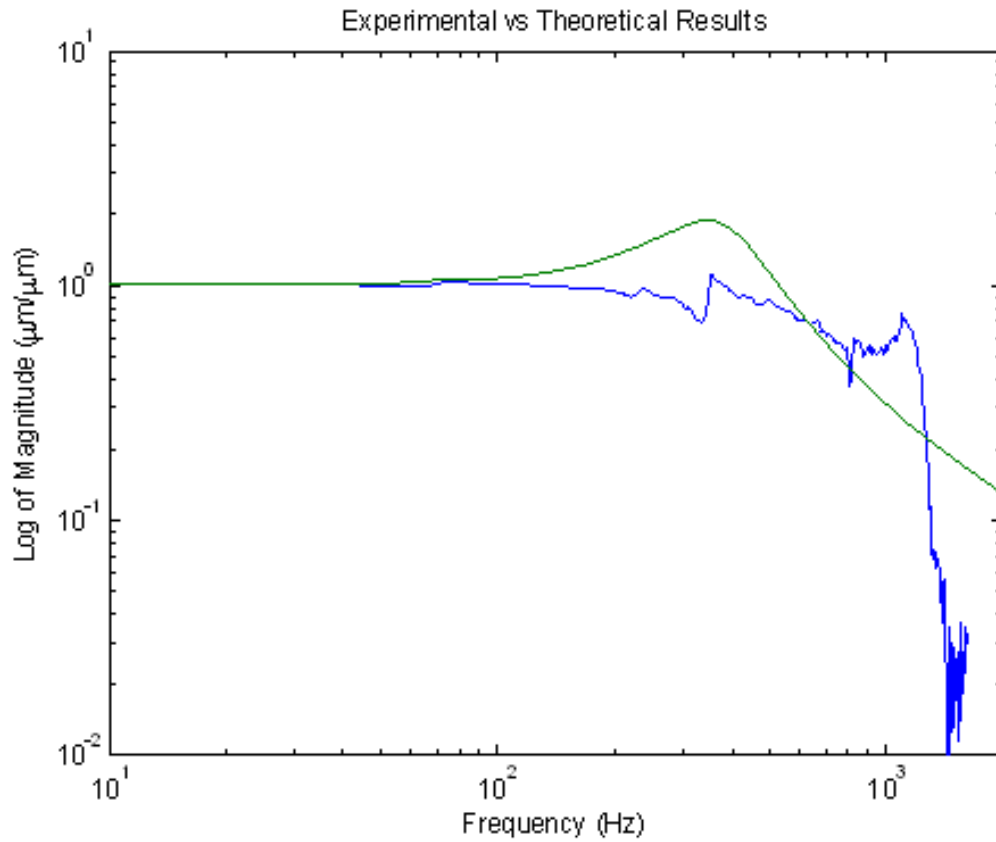
Figure 2.7: Magnitude Plot of the Experimental and Theoretical Results using Second-Order Model

A third test was done of the PCB MEMS accelerometer. The test set-up used a reference accelerometer as an input and the output voltage from the PCB MEMS accelerometer as the output. The electromechanical shaker was excited at random frequencies in the range of 10-1600 Hz. The test results are shown in Figure 2.8. The results show a linear ratio between the output voltage and the input acceleration for a given frequency. At the resonant frequency (375 Hz), for an input acceleration of 1 g an output of approximately 4 mV is given. The accelerometer should be operated in the low-frequency range (30-400 Hz) where

the curve is mostly flat in order for the accelerometer to give consistant results over the range.

Figure 2.8: Magnitude Plot of the Transfer Function for the PCB MEMS Accelerometer (Third Test, Electrical Response)

2.3   System Identification

The experimental data is examined in a control systems analysis technique known as system identification. MATLAB's System Identification Toolbox was used to develop some higher-order models to fit the experimental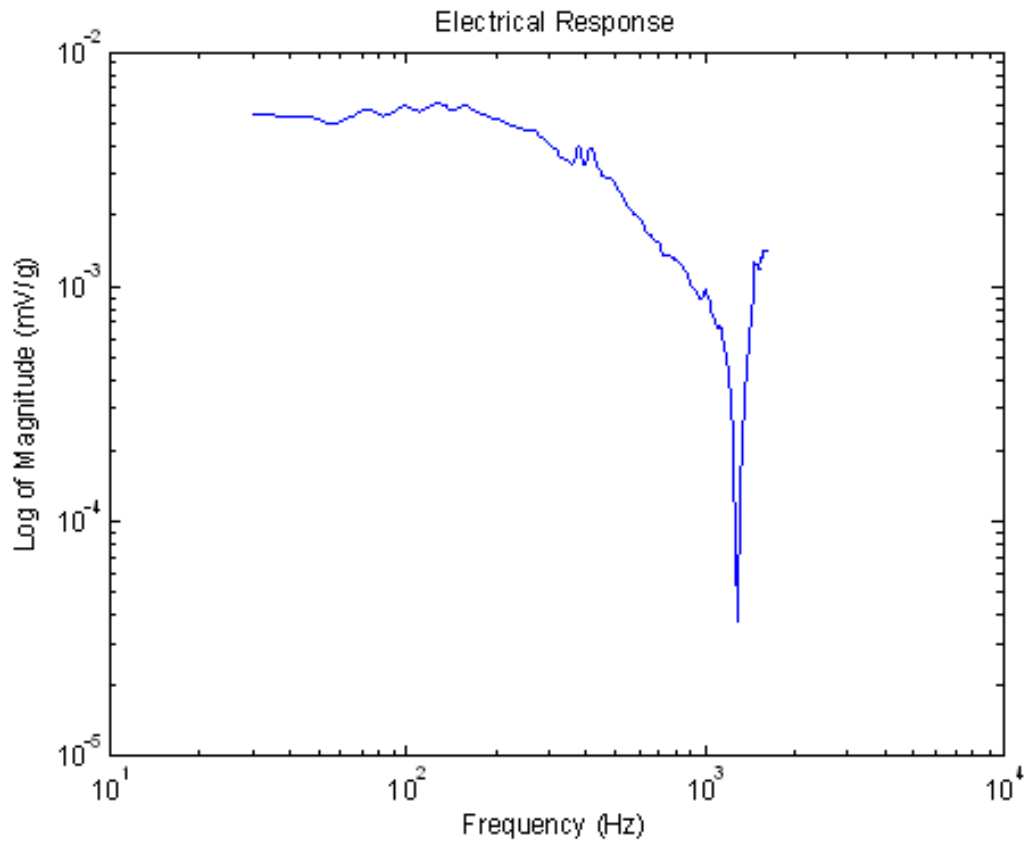 data in order to get an insight into the relative order of the system. The System Identification Toolbox is brought up in a GUI window of MATLAB's command window using the 'Ident' command. The GUI program allows the user to import time domain or frequency domain experimental data. The experimental data used was one of the mechanical response plots from the second test (Figure 2.9). The System Identification Toolbox has three methods for estimating models: parametric estimation, process model estimation, and nonparametric estimation. The parametric estimation method was chosen due to its ability to allow the user to select the order of the polynomial for the transfer function. The user then has the ability to select the number of poles, zeros, and time delays.

In Figure 2.10 a transfer function with four poles, three zeros, and one delay was estimated to fit the experimental data curve. The curve seems to look like a second-order response, but having a resonant peak at the second resonant point. In Figure 2.11 a transfer function with eight poles, six zeros, and three delays is shown. The curve fits better with the experimental data and even seems to show the first resonant peak, but doesn't show the dip before the first resonant peak. In Figure 2.12 a transfer function with eight poles, seven zeros, and one delay is shown. The curve fits really well with the experimental data showing the first and second resonant points, and the dip before the first resonant point.

Although MATLAB's System Identification Toolbox can be used to develop higher-order models it is important to have a controls background to interpret the data. All three

of the generated transfer functions by MATLAB were unstable in discrete time showing zeros and poles outside the unit circle. It is uncertain how MATLAB does numerically analysis of the experimental data and many of the coefficients are extremely large which could lead to the stability issues. A controls background can allow one to estimate the system order by pole-zero placement using classical control system techniques [13]. A fourth order system was estimated by placing two pairs of complex poles at the resonant points and a pair of complex zeros at the dip before the first resonant point. The placed pole-zero system is shown in Figure 2.13. The system matches the experimental data pretty well for a quick estimate. The conclusion can be made by observing these models that the system is in fact higher-order. A second-order model gives a pretty good estimate, but a higher-order model gives a much better estimate of the actual system.

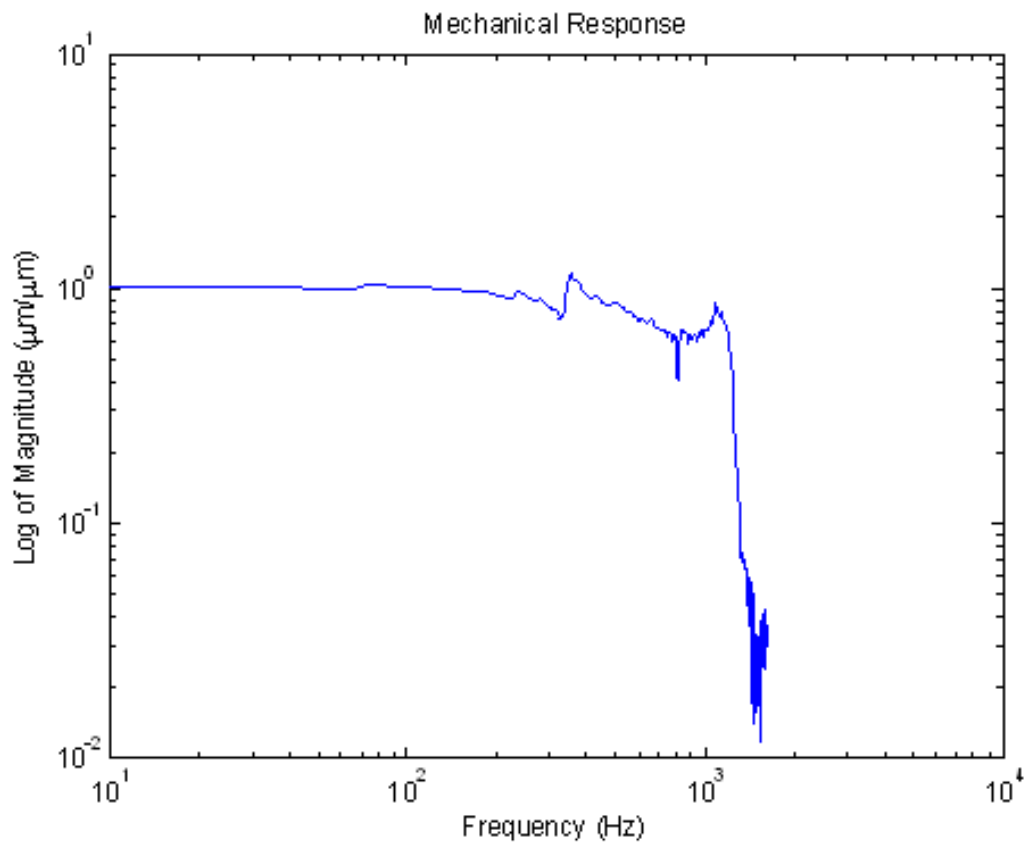Figure 2.9: Magnitude Plot of the Transfer Function for the PCB MEMS Accelerometer (Second Test, Mechanical Response)
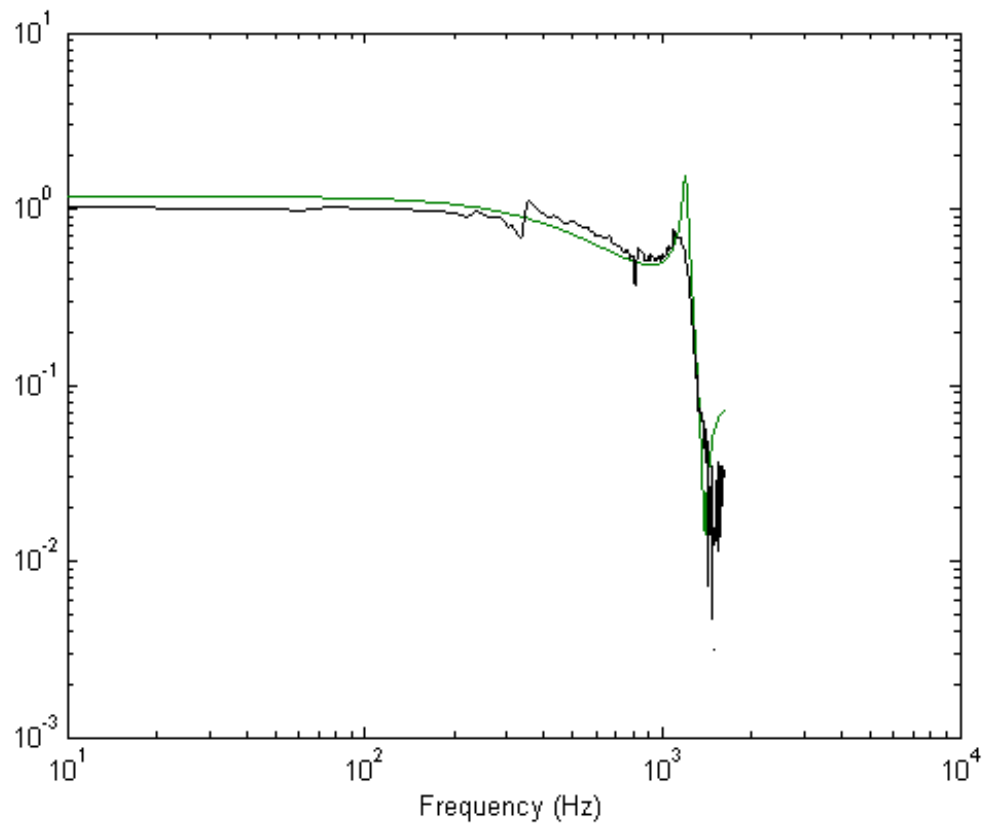
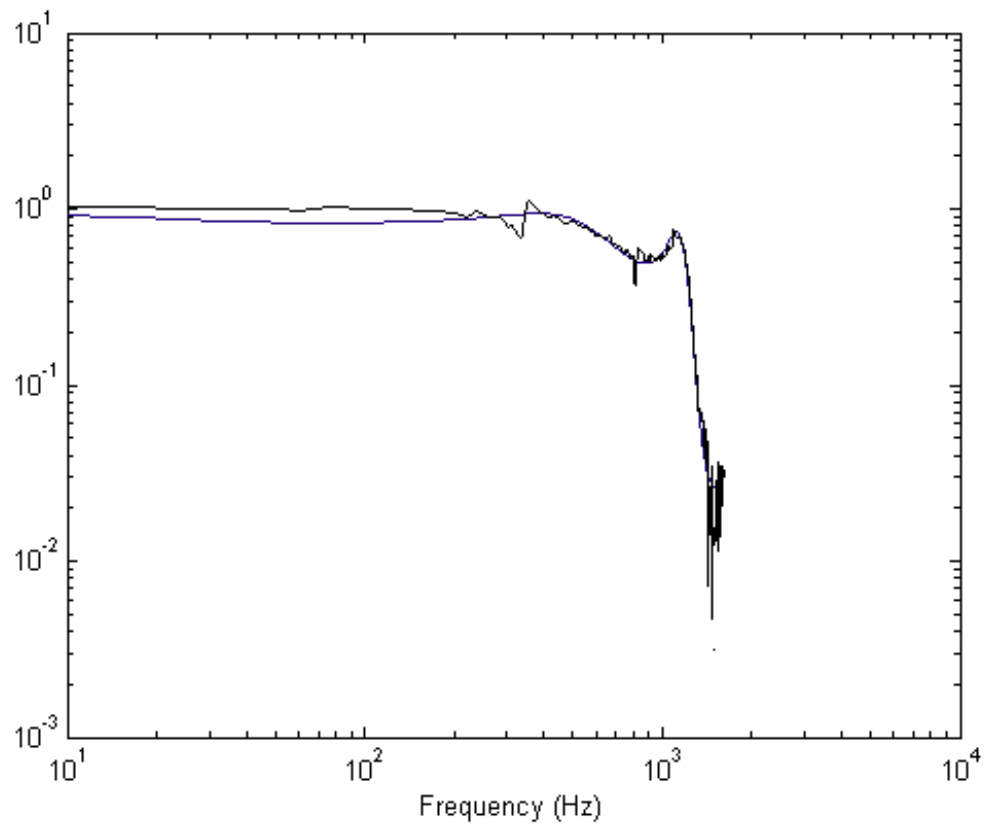Figure 2.10: Four pole, three zero, one delay transfer function (MATLAB SYSID)

Figure 2.11: Eight pole, six zero, three delay transfer function (MATLAB SYSID)
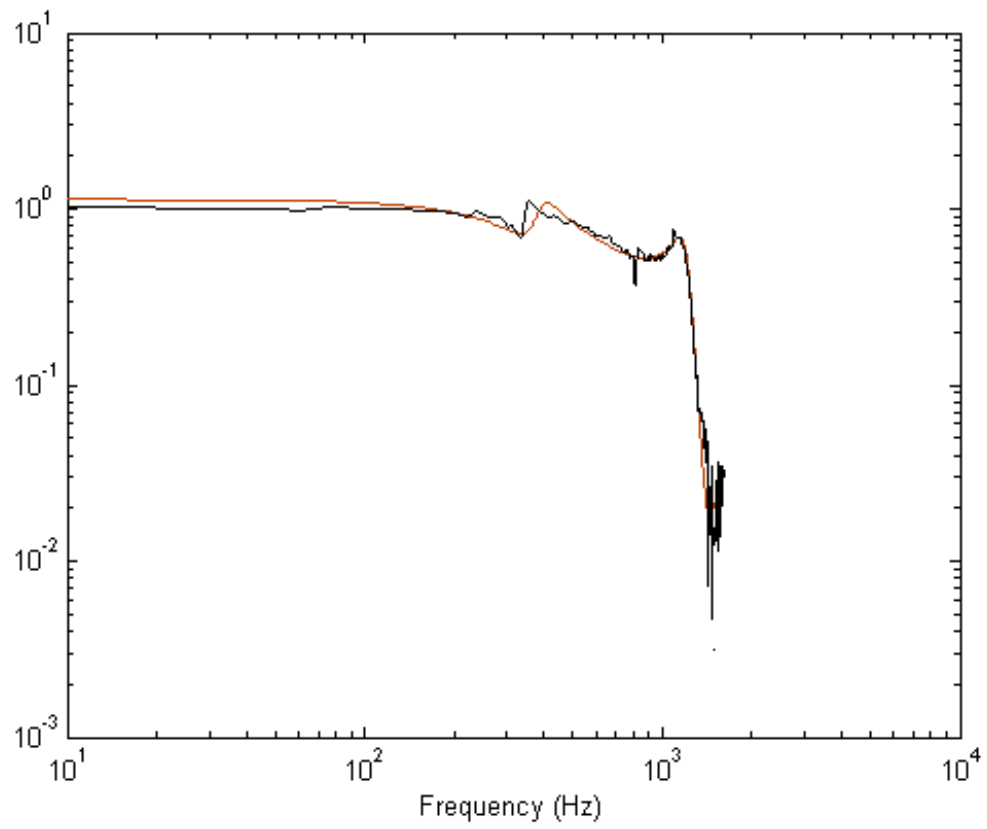
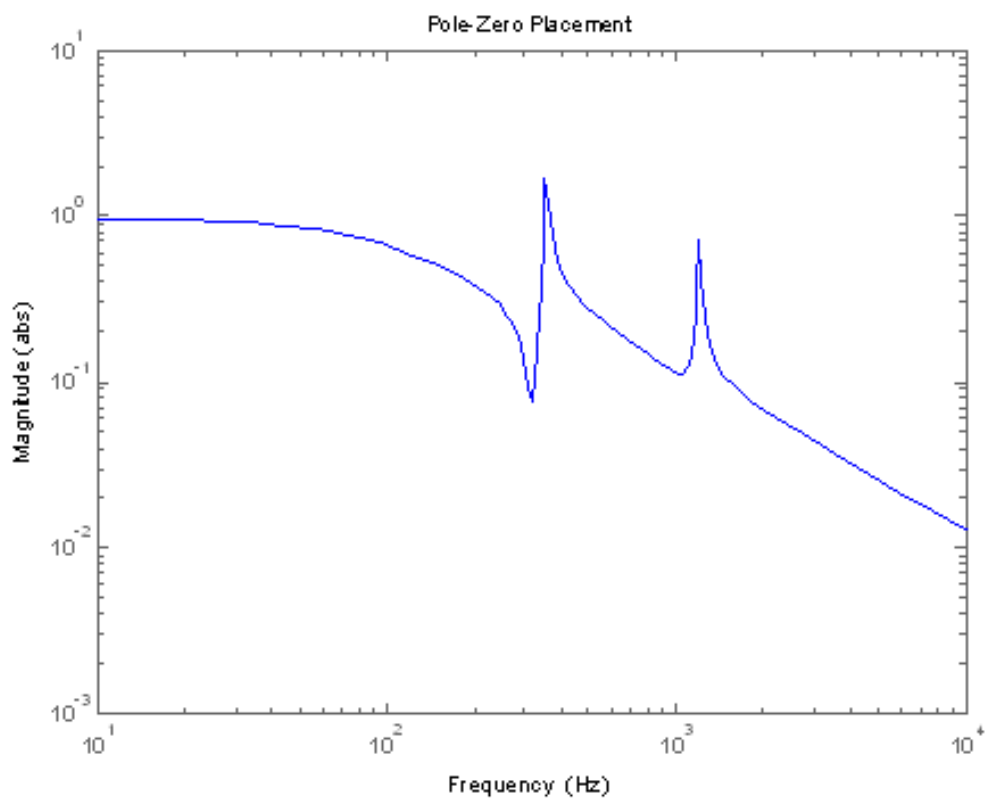Figure 2.12: Eight pole, seven zero, one delay transfer function (MATLAB SYSID)

40

Figure 2.13: Fourth order pole-zero placement transfer function

CHAPTER 3

CONCLUSIONS & FUTURE WORK

3.1 Il Buono

A MEMS-based accelerometer was fabricated using printed circuit processing techniques. The design, fabrication, and mechanical characterization of the PCB MEMS accelerometer were discussed. The resonant frequency of an example accelerometer with a square membrane of area 6.4 mm×6.4 mm was measured to be 375 Hz. The attractive feature of PCB MEMS is that it enables monolithic integration of MEMS devices with electronics using conventional printed circuit techniques. The advantages of the proposed PCB MEMS technology include low-cost, ease of integration with electronics, suitability for high-volume manufacturing, and large area applications.

3.2 Il Brutto

The experimental results of the fabricated MEMS accelerometer show that some of the actual parameters didn't match well with the designed parameters. This is largely due to the two issues: 1) excess copper on the plate that increased the stiffness of the springs, and 2) the large gap increase due to thermal expansion of copper and Kapton®. More devices should be fabricated using other fabrication techniques to try to eliminate this large gap change. The fabrication of PCB MEMS devices is still at the experimental stage and a single technique hasn't been developed for various devices thus many tests must be done to refine the process for any one device.

3.3 Il Cattivo

The experimental results of the fabricated MEMS accelerometer show a higher-order model than the predicted second-order model. This is most likely due to the fact that the structure is flexible. Fabrication of smaller square plates should be done to see if/when the structure will become rigid. Every rigid structure has a point where it becomes flexible due to the large surface area to thickness ratio and material properties. It was not hypothesized that the MEMS accelerometer would be flexible.

3.4 Future Work

The new hypothesis now accepts that the structure is flexible and the new question is to what size will the device become rigid. The ability to have a rigid structure will allow for lumped-element modeling of the MEMS accelerometer. The need to conduct tests on multiple devices of the same geometry, but different sizes will help to provide better statistical data on the performance of PCB MEMS accelerometers and how they behave. Lastly, someone should look into applying the science of flexible structures to the modeling of PCB MEMS. This would give further insight into better predicting the behavior of the system.

BIBLIOGRAPHY

[1] B. Borovic, F. L. Lewis, W. McCulley, A. Q. Liu, E. S. Kolesar, and D. O. Popa, "Control issues for microlectromechanical systems," *IEEE Control Systems Magazine*, vol. 26, pp. 18–21, April 2006.

[2] E. Bryzek, A. Abbott, D. C. Flannery, and J. Maitan, "Control issues for mems," *IEEE Conf. Decision and Control*, vol. 3, pp. 3039–3047, 2003.

[3] C. T.-C. Nguyen, "Frequency-selective mems for miniaturized low-power communication devices," *IEEE Transactions on Microwave Theory and Techniques*, vol. 47, pp. 1486–1503, August 1999.

[4] J. Rogers, P. Ozmun, J. Hung, and R. Dean, "Bi-directional gap closing mems actuator using timing and control techniques," *Proceedings of the 32nd Annual Conference of the IEEE Industrial Electronics Society (IECON'06)*, pp. 3149–3154, November 2006.

[5] R. Ramadoss, S. L. S, Y. Lee, V. Bright, and K. Gupta, "Rf mems capacitive switches fabricated using printed circuit processing techniques," *IEEE/ASME Journal of Microelectromechanical Systems*, vol. 15, pp. 1595–1604, December 2006.

[6] X. Wang, J. Engel, and C. Liu, "Liquid crystal polymer (lcp) for mems: processes and applications," *J. Micromech. Microeng.*, vol. 13, pp. 628–633, 2003.

[7] J. N. Palasagaram and R. Ramadoss, "Mems capacitive pressure sensor fabricated using printed circuit processing techniques," *IEEE Sensors Journal*, vol. 6, pp. 1374–1375, December 2006.

[8] D. Fries, G. Steimle, S. Natarajan, S. Ivanov, H. Broadbent, and T. Weller, "Maskless lithography pcb/laminate mems for a salinity sensing system," *Proc. Int. Microelectron. Packag. Soc. (IMAPS) Workshop on Packag. MEMS and Related Micro Integr./Nano Syst.*, 2002.

[9] R. Jackson and R. Ramadoss, "A mems-based electrostatically tunable circular microstrip patch antenna," *Journal of Micromechanics and Microengineering*, vol. 17, pp. 1–8, January 2007.

[10] J. Soderkvist, "Similarities between piezoelectric thermal and other internal means of exciting vibrations," *Journal of Micromechanics and Microengineering*, vol. 3, pp. 24–31, 1983.

[11] M.-H. Bao, *Micro Mechanical Transducers: Pressure Sensors, Accelerometers and Gyroscopes*, vol. 8. New York: Elsevier Science, 2000.

[12] R. Jackson, "Mems based tunable microstrip patch antenna fabricated using printed circuit processing techniques," Master's thesis, Auburn University, August 2006.

[13] R. C. Dorf and R. H. Bishop, *Modern Control Systems*. Prentice Hall, 10 ed., 2004.
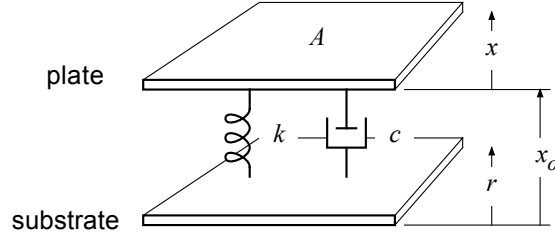
RIGID BODY MODEL FOR MEMS ACCELEROMETER

Figure A.1: Cross-sectional view of PCB MEMS device

Shown above in Figure A.1 is a spring-mass-damper rigid body model for a typical MEMS accelerometer. The system has two plates, a top plate and the substrate. The plate area is defined by A. The spring constant for the system is k, the damping constant for the system is c, and the nominal gap distance between the two plates is x_o. When an external force is applied to the substrate, a displacement r is seen and results in a displacement of the top plate given by x. The electrical and mechanical dynamics for the spring-mass-damper are described as follows:

A.1 Electrical Dynamics

The capacitance for a parallel plate capacitor is given by

$$C = \frac{\epsilon A}{x_o - x} \tag{A.1}$$

Through the charge-voltage relationship

$$q = Cv = \frac{\epsilon A v}{x_o - x} \tag{A.2}$$

The work is defined by

$$W = \frac{qv}{2} = \frac{\epsilon A v^2}{2} \left(\frac{1}{x_o - x} \right) \tag{A.3}$$

The electrostatic force is the change in work

$$F_e = \frac{\partial W}{\partial x} = \frac{\epsilon A}{2} \left(\frac{v}{x_o - x} \right)^2 \tag{A.4}$$

where ϵ is the permittivity of the surrounding gas, A is the plate area, v is the applied voltage, and x_o is the nominal gap distance.

A.2 Mechanical Dynamics

The inertia force, also known as Newton's second law

$$F_{inertia} = m\ddot{x} \tag{A.5}$$

The damping force

$$F_{damper} = -c(\dot{x} - \dot{r}) \tag{A.6}$$

47

The spring force, also known as Hooke's Law

$$F_{spring} = -k(x - r) \tag{A.7}$$

The mechanical force is the sum of the inertia, damper, and spring forces

$$F_m = F_{inertia} + F_{damper} + F_{spring} \tag{A.8}$$

The differential equation for the mechanical force is thus

$$F_m = m\ddot{x} + c\dot{x} + kx \tag{A.9}$$

where m is the proof mass, $\ddot{x}$ is the acceleration of the plate mass, c is the damping constant, $\dot{x}$ is the velocity of the plate mass, $\dot{r}$ is the velocity of the substrate, k is the spring constant, x is the displacement of the plate mass, and r is the displacement of the substrate.

Equating the mechanical and electrical dynamic force equations yields a stable state thus producing an electromechanical model for the MEMS accelerometer

$$m\ddot{x} = -c\dot{x} - kx + \frac{\epsilon A}{2}\left(\frac{v}{x_o - x}\right)^2 \tag{A.10}$$

48

A.3 Mechanical Transfer Function

$$m\ddot{x} + c(\dot{x} - \dot{r}) + k(x - r) = 0 \tag{A.11}$$

$$ms^2 X(s) + csX(s) - csR(s) + kX(s) - kR(s) = 0 \tag{A.12}$$

$$(ms^2 + cs + k)X(s) = (cs + k)R(s) \tag{A.13}$$

$$\frac{X(s)}{R(s)} = \frac{(cs + k)}{ms^2 + cs + k} \tag{A.14}$$

one zero at

$$s = -\frac{k}{c} \tag{A.15}$$

two poles at

$$s = \frac{-c \pm \sqrt{c^2 - 4mk}}{2m} \tag{A.16}$$

Rayleigh-Ritz Method for Determining Equivalent Mass of a Flexible Structure
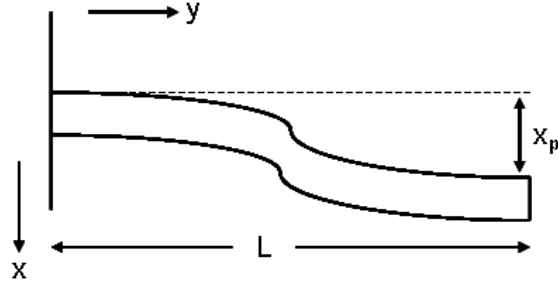
Figure B.1: Shape Function for Suspension Beam

Shown above in Figure B.1 is the shape function for a suspension beam. The length of the beam is given by L. The maximum displacement due to a force is given by x_p.

The shape function for a suspension beam is given by

$$x_b(y) = x_p \left[3(\frac{y}{L})^2 - 2(\frac{y}{L})^3 \right] \tag{B.1}$$

The maximum potential energy

$$E_{pmax} = \frac{1}{2} k x_p^2 \tag{B.2}$$

The maximum kinetic energy

$$E_{kmax} = \frac{1}{2} \left[v_p^2 m_p + \int v_b^2 dm_b \right] \tag{B.3}$$

The change in mass can be re-expressed $dm_b = m_b \frac{dy}{L}$

$$E_{kmax} = \frac{1}{2}v_p^2 m_p + \frac{1}{2}\int v_b^2 m_b \frac{dy}{L} \tag{B.4}$$

The velocity can be re-expressed $v = \omega x$

$$E_{kmax} = \frac{1}{2}x_p^2\omega_n^2 m_p + \frac{1}{2L}m_b\int (\omega_n x_b)^2 dy \tag{B.5}$$

Substituting for x_b

$$E_{kmax} = \frac{1}{2}x_p^2\omega_n^2 m_p + \frac{1}{2L}m_b\int \left(\omega_n x_p \left[3(\frac{y}{L})^2 - 2(\frac{y}{L})^3\right]\right)^2 dy \tag{B.6}$$

Re-writing the kinetic energy equation

$$E_{kmax} = \frac{1}{2}x_p^2\omega_n^2 \left[m_p + \frac{13}{35}m_b\right] \tag{B.7}$$

By the principle of energy conservation

$$E_{pmax} = E_{kmax} \tag{B.8}$$

Equating the kinetic and potential energy

$$\frac{1}{2}kx_p^2 = \frac{1}{2}x_p^2\omega_n^2 \left[m_p + \frac{13}{35}m_b\right] \tag{B.9}$$

The resonant frequency as a function of effective spring constant and proof mass

$$\omega_n^2 = \left[\frac{k}{m_p + \frac{13}{35}m_b} \right] \tag{B.10}$$

The effective proof mass is thus

$$m = m_p + \frac{13}{35}m_b \tag{B.11}$$

where m_p is the plate mass and m_b is the beam mass.

The plate and beam masses are given by

$$m_p = \rho V_p \tag{B.12}$$

$$m_b = \rho V_b \tag{B.13}$$

APPENDIX C

LINEAR STATE VARIABLE ANALYSIS FOR PCB MEMS ACCELEROMETER

C.1 Motivation

Electrostatic Micro-Electro Mechanical Systems, or MEMS, are an interesting problem in control systems in that they tend to have second-order nonlinear system dynamics that resemble those of mass-spring-damper systems with a capacitive-like structure. If a structure is rigid the following could be used to design a feedback control system. The objective is to design a control system that stabilizes the output $y = x$, the actuator position.

C.2 Dynamic Model

Dynamics of the PCB MEMS Accelerometer are described by the nonlinear ordinary differential equation

$$m\ddot{x} = -c\dot{x} - kx + \frac{\epsilon_o A V^2}{2} \frac{1}{(x_o - x)^2} \tag{C.1}$$

Electrostatics of the PCB MEMS Accelerometer are described by the nonlinear equation

$$kx = \frac{\epsilon_o A V^2}{2} \frac{1}{(x_o - x)^2} \tag{C.2}$$

Let $m = 4.375 \times 10^{-6}$ kg, $c = 6.7 \times 10^{-3}$ N-sec/m, $k = 24.791$ N/m, $A = 34.34$ mm^2, and $x_o = 125$ μm.

C.3   State Variables

Let the state be

$$z = \begin{bmatrix} x \\ \dot{x} \end{bmatrix}$$

The plant input is $u = V$, and there is one output. Rewriting dynamic equation C.1 in state variable form

$$\dot{z} = f(z, u) \tag{C.3}$$

$$y = h(z) \tag{C.4}$$

$$\dot{z}_1 = z_2$$

$$\dot{z}_2 = -\frac{c}{m}z_2 - \frac{k}{m}z_1 + \frac{\epsilon_o AV^2}{2m}\frac{1}{(x_o - z_1)^2}$$

C.4   Equilibrium State

The equilibrium state z_e, u_e can be determined by observing the position versus applied voltage graph (Figure C.1) for the electrostatic equation C.2.

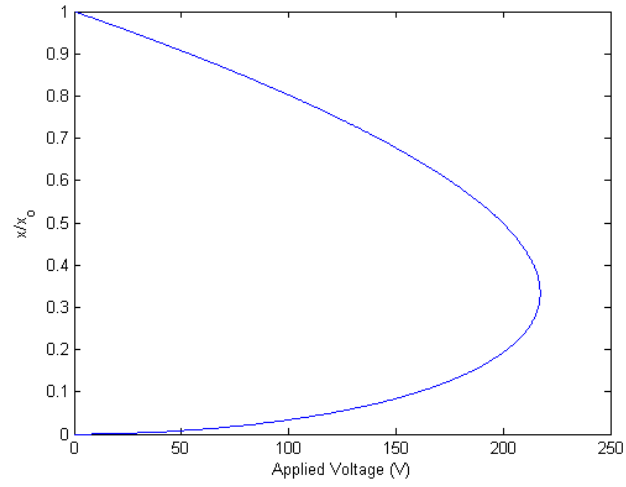The chosen equilibrium point satisfies equation C.2 $z_e = [10.5 \times 10^{-6} \ 0]$, $u_e = [150]$.

Figure C.1: Normalized pull-down voltage curve

C.5 Linearized State Variable Model

Find the linearized state variable model of the form

$$\dot{\delta z} = A\delta z + B\delta u \tag{C.5}$$

$$\delta y = C\delta z \tag{C.6}$$

where $\delta z = z - z_e$ and $\delta u = u - u_e$.

Recall that there is one output variable, $y = x$.

$$A = \nabla_z f|_{z_e,u_e} = \begin{bmatrix} 0 & 1 \\ -\frac{k}{m} + \frac{\epsilon_o A V^2}{m}\frac{1}{(x_o-z_1)^3} & -\frac{c}{m} \end{bmatrix}_{z_e,u_e}$$

$$A = \begin{bmatrix} 0 & 1 \\ -4.6 \times 10^6 & -1532 \end{bmatrix}$$

$$B = \nabla_u f|_{z_e, u_e} = \begin{bmatrix} 0 \\ \frac{\epsilon_o AV}{m} \frac{1}{(x_o - z_1)^2} \end{bmatrix}_{z_e, u_e}$$

$$B = \begin{bmatrix} 0 \\ 0.80 \end{bmatrix}$$

$$C = \nabla_z h|_{z_e, u_e} = \begin{bmatrix} 1 & 0 \end{bmatrix}_{z_e, u_e} = \begin{bmatrix} 1 & 0 \end{bmatrix}$$

C.6   Stability

Analyze stability of the linear state variable model (C.5), (C.6).

$$\delta \dot{z}_1 = z_2$$

$$\delta \dot{z}_2 = -5.6 \times 10^6 z_1 + 119.3 - 1532 z_2 + 0.80u$$

Assume a positive-definite Lyapunov function

$$V(z) = z_1^2 + 2z_1 z_2 + z_2^2$$

$$\frac{d}{dt} V(z) = (\nabla_z V)\dot{z}$$

$$\nabla_z V = \begin{bmatrix} 2z_1 + 2z_2 & 2z_1 + 2z_2 \end{bmatrix}$$

The function $\dot{V}(z)$ is negative-definite and thus solutions for $\dot{z}$ are asymptotically stable.

C.7 Controllability

$$rank \begin{bmatrix} B & AB \end{bmatrix} = 2 = dim(z)$$

The rank of (A, B) is equal to the dimension of z, thus the system is controllable.

C.8 Observability

$$rank \begin{bmatrix} C \\ CA \end{bmatrix} = 2 = dim(z)$$

The rank of (A, C) is equal to the dimension of z, thus the system is observable.

C.9 Stabilizability

$$|sI - A| = \begin{vmatrix} s & -1 \\ 4.6 \times 10^6 & s + 1532 \end{vmatrix} = s^2 + 1532s + 4.6 \times 10^6 = 0$$

$$s = -766 \pm 2003i$$

The system is naturally stable, thus it is stabilizable.

C.10 Detectability

The system is naturally stable, thus it is stabilizable and detectable, also controllable and observable.

C.11 Linear State Feedback

A linear state feedback $\delta u = -K \delta z$ is to be designed to place eigenvalues of $(A - BK)$ at $-800 \pm j800$.

$$
A - BK = A_C = \begin{bmatrix} 0 & 1 \\ -4.6 \times 10^6 - 0.80K_1 & -1532 - 0.80K_2 \end{bmatrix}
$$

$$
|sI - (A - BK)| = \begin{vmatrix} s & -1 \\ 4.6 \times 10^6 + 0.80K_1 & s + 1532 + 0.80K_2 \end{vmatrix}
$$

$$
= s^2 + (1532 + 0.80K_2)s + (4.6 \times 10^6 + 0.80K_1) = 0
$$

desire $s = -800 \pm j800$

$$
(s + 800)^2 + (800)^2 = s^2 + 1600s + 128 \times 10^4 = 0
$$

$$
K_1 = -4.15 \times 10^6, K_2 = 85
$$

$$
K = \begin{bmatrix} K_1 & K_2 \end{bmatrix} = \begin{bmatrix} -4.15 \times 10^6 & 85 \end{bmatrix}
$$

C.12 Observer Gain

An observer gain L is to be designed so that the estimation error dynamics are characterized by the eigenvalues $-900 \pm j900$.

$$A - LC = A_O = \begin{bmatrix} -L_1 & 1 \\ -4.6 \times 10^6 - L_2 & -1532 \end{bmatrix}$$

$$|sI-(A-LC)| = \begin{vmatrix} s + L_1 & -1 \\ 4.6 \times 10^6 + L_2 & s + 1532 \end{vmatrix} = s^2+(1532+L_1)s+(4.6\times10^6+1532L_1+L_2) = 0$$

desire $s = -900 \pm j900$

$$(s + 900)^2 + (900)^2 = s^2 + 1800s + 162 \times 10^4 = 0$$

$$L_1 = 268, L_2 = -3.39 \times 10^6$$

$$L = \begin{bmatrix} L_1 \\ L_2 \end{bmatrix} = \begin{bmatrix} 268 \\ -3.39 \times 10^6 \end{bmatrix}$$

C.13 Simulation

Simulate the closed loop behavior of the nonlinear system (C.3) under the linear state feedback control designed in Section C.5. Let the initial condition be $z(0) = [0.5 \times 10^{-6} \ 0]^T$. Plot the time response of the GCA position x.

Simulate the closed loop behavior of the nonlinear system (C.3) under the estimated state feedback control $\delta u = -K\delta\hat{z}$. Use the observer designed in Section C.6. Let the initial
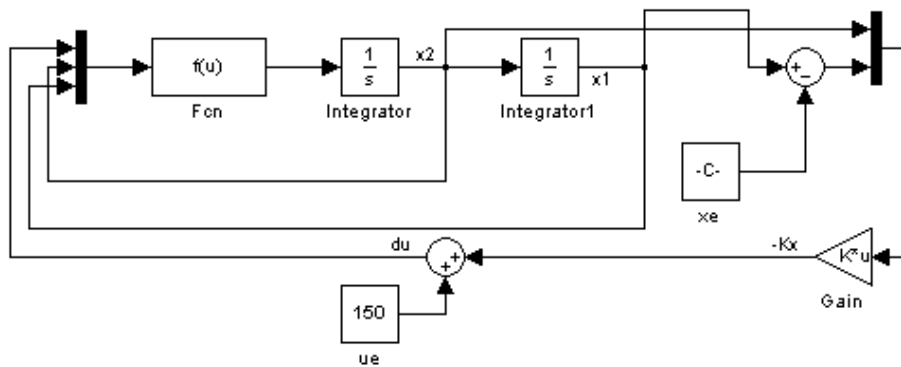
Figure C.2: Block diagram for linear state feedback control

condition be $z(0) = [0.5 \times 10^{-6}\ 0]^T$, and the initial value of the estimated state be $\delta\hat{z} = [0\ 0]^T$. Plot the time response of the GCA position x. Plot the estimation error $x - \hat{x}$.

Since the damping in the problem is so small relative to the mass, increasing the damping constant, c, would allow for better control. This is not usually an easy thing to do, but by isolating the device within the right gas and pressure would do just this. The system is naturally a very stiff system and controlling the damping will thus allow for better control of K and L.
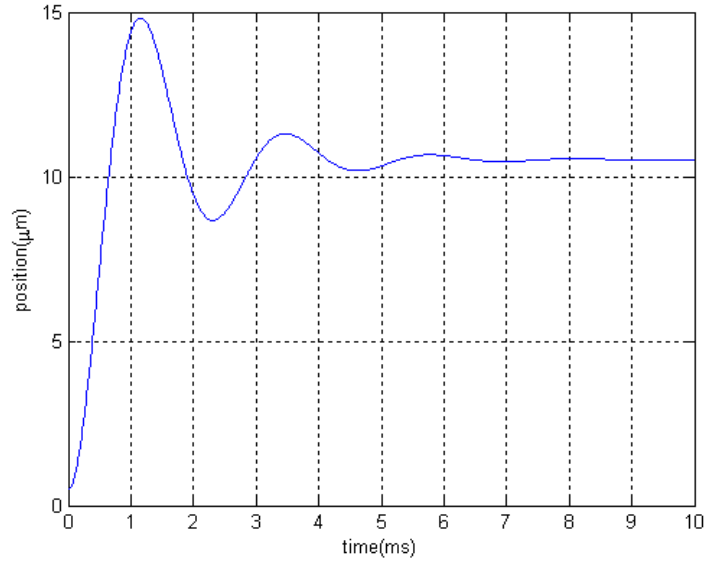
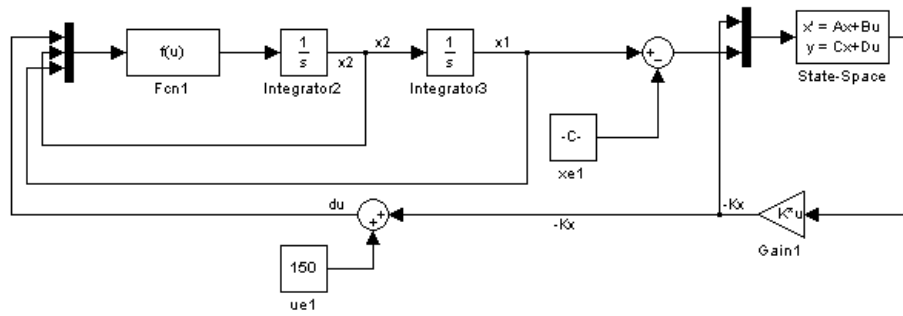Figure C.3: Output response for linear state feedback control

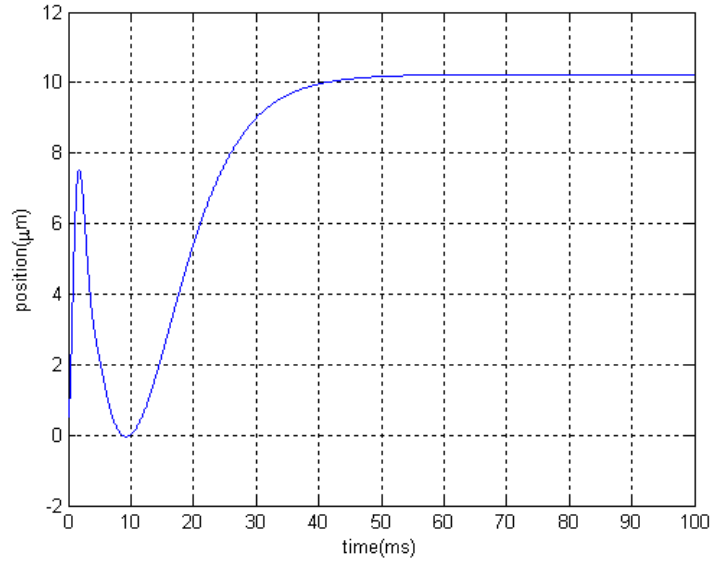Figure C.4: Block diagram for estimated state feedback control

61

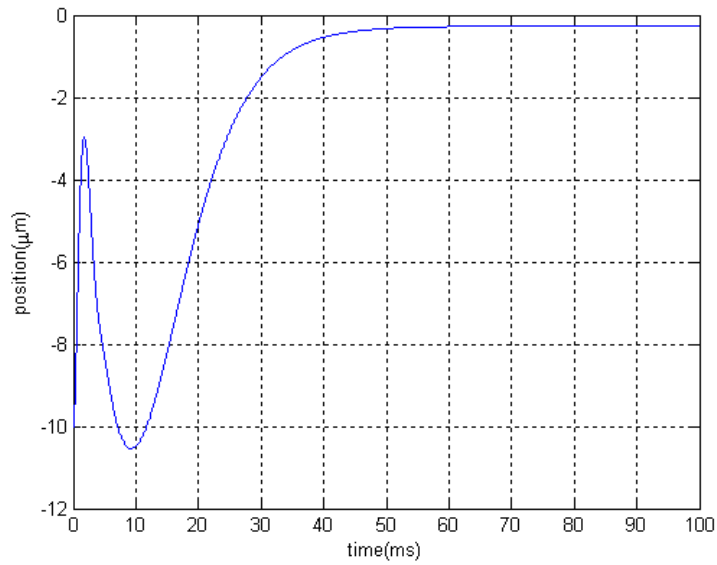Figure C.5: Output response for estimated state feedback control

Figure C.6: Estimation error for estimated state feedback control

MATLAB CODE

```matlab
% John Rogers
% Auburn University
% PCB MEMS Accelerometer Design
clc
format compact

%Kapton/Copper Material Properties
E_k=780*6894757;                %Pa
E_c=124.8*10^9;                 %Pa
t=50.8e-6;                      %m (50.8um)
t_c=3e-6;                       %m (3um)
rho_k=1420;                     %kg/m^3
rho_c=8960;                     %kg/m^3

%Beam Design Parameters
l=5.8e-3;                       %m (5.8mm)
w=1e-3;                         %m (1mm)

%Mass Design Parameters (square mass)
d=6.4e-3;                       %m (6.4mm)
rc=270e-6;                      %m (270um)
d_c=d-2*rc                      %m

%Beam Stiffness (4 fixed-fixed in parallel)
w_c = 100e-6;                   %m (100um)
EI = ((w*E_k*t^2)^2+(w_c*E_c*t_c^2)^2+2*w*w_c*E_k*E_c*t*t_c*...
(2*t^2+3*t*t_c+2*t_c^2))/(12*(w*E_k*t+w_c*E_c*t_c));
k = 48*EI/l^3
```

Figure D.1: PCB MEMS Accelerometer Parameters MATLAB Code

```matlab
%Proof Mass (kapton and copper)
m_k=d^2*t*rho_k;                    %kg
m_c=d_c^2*t_c*rho_c;               %kg
m=m_k+m_c +4*13/35*l*w*t*rho_k    %kg

%Initail Capacitance Gap, Capacitance Area
eo=8.854e-12                       %F/m
g=41.8e-6                          %m (41.8um) **(50.8um - 9um)
A_c=d_c^2                          %m^2

%Natural Frequency, Sensitivity, Capacitance
omega=sqrt(k/m)                    %rad/s
Sen=1/omega^2                      %s^2

a=0:.5:50;                         %m/s^2
dis=a*Sen;                         %m
C=(g-dis).^-1*eo*A_c*10^12;        %pF

%Damping & Q-Point
mu = 1.827e-5;                     %pa.s
c_sf = .42*mu*d*d^3/g^3+4*mu*l*w^3/g^3
Q = omega*m/c_sf

plot(a,C)
title('Capacitance vs Acceleration')
xlabel('Acceleration (m/s^2)')
ylabel('Capacitance (pF)')
```

Figure D.2: PCB MEMS Accelerometer Paramaters MATLAB Code (Cont.)